

POLITECNICO DI MILANO

School of Industrial and Information Engineering

Master of Science in Automation and Control Engineering



POLITECNICO
MILANO 1863

Improving the comfort of a motorcycle using a multichamber suspension

Supervisor: Prof. Sergio Savaresi

Co-supervisor: Prof. Matteo Corno

Prof Giulio Panzani

Tutor: Ing. Stefano Dattilo

Master Thesis dissertation of:
Mohammed Aadil Ahmed Matr. 895437

Accademic year 2019-2020

Acknowledgements

Thanks to God, for giving me the opportunity to be part of this university and amazing program.

Thanks to my family, who have supported me emotionally, financially and mentally throughout my journey in acquiring knowledge and becoming a better person.

Thanks to Professor Savaresi, for doing a phenomenal job in teaching me the course automation and control in vehicles, and igniting the passion to pursue research in this domain.

Thanks to Professor Corno and Professor Panzani, for taking the time to patiently discuss during meetings and helping me out throughout the thesis.

Thanks to Stefano, who has been one of the best advisors to me in my life. I have learned a great deal both technically and non-technically from him.

Thanks to Albino, who has been my best friend to me in university and being by my side during my toughest moments.

Contents

Abstract	1
1 Introduction	5
1.1 Scope of Interest	7
1.2 Main Contribution	8
1.2.1 Passive suspension design and analysis	8
1.2.2 Multichamber sizing	8
1.2.3 Optimization result	11
1.3 Structure of the Thesis	12
2 State of art	13
2.1 Variable stiffness technologies	13
2.1.1 Horizontal strut based passive variable stiffness	13
2.1.2 Magnetic suspension system	15
2.1.3 Damper based variable stiffness	15
2.1.4 MR (magnetorheological) elastomer isolator	17
2.1.5 Multichamber suspension	18
2.2 Algorithms using Variable stiffness	19
2.2.1 Stroke Speed Threshold Stiffness Control (SSTSC)	19
2.2.2 Double Stroke Threshold Stiffness Control (DSTSC)	19
2.2.3 Stiffness and damping control to reduce dynamical effects .	20
2.3 Conclusion	21

3 Simulation setup	22
3.1 Motorcycle simulator	22
3.1.1 Masses and moment of inertias in the simulator	22
3.1.2 Dimensions of the motorcycle	24
3.1.3 Stiffness and damping elements	24
3.1.4 Rear wheel jounce and stroke relationship	27
3.1.5 Derivative of sensor speed	30
3.1.6 Road profile	30
3.2 Multichamber suspension model	32
3.3 Comfort cost function	35
4 Passive sensitivity analysis	36
4.1 Front suspension sensitivity	36
4.2 Rear suspension sensitivity	41
4.3 Effect of damping on longitudinal dynamics	46
4.4 Conclusion	46
5 Multichamber sizing	47
5.1 Model	47
5.2 Sizing objective	47
5.3 Equations of the multichamber suspension	48
5.4 Parameters sensitivity	49
5.5 2 state stiffness selection	50
5.6 Sizing results	51
5.6.1 Comparing sizing with a real suspension	52
5.7 Conclusion	53
6 Brute-force optimization	54
6.1 Brute-force optimization algorithm	54
6.1.1 Optimization conditions	56

CONTENTS	vii
6.2 Optimization results	56
6.3 Contribution of vertical and pitch acceleration improvement . . .	59
6.4 Conclusion	60
7 Conclusion	63
Bibliography	66

List of Figures

1.1	Cross-sectional view of a real Porche multichamber suspension.	6
1.2	Sketch view of the Porche multichamber suspension.	6
1.3	Rear suspension sensitivity with vertical cost function.	9
1.4	Front suspension sensitivity with vertical cost function.	9
1.5	Multichamber suspension dimensions.	10
1.6	2 state optimization sensitivity using J_{tot} cost function.	11
2.1	Strut based Passive variable stiffness technology.	14
2.2	Strut based Passive variable stiffness technology (schematic).	14
2.3	Schematic of magnetic suspension system.	15
2.4	Stiffness vs current graph for magnetic suspension system.	16
2.5	Variable stiffness based on modulating damper.	16
2.6	Variable damper.	17
2.7	MRE schematic.	17
2.8	Current sensitivity for MRE technology.	18
2.9	Stroke Speed Threshold Stiffness Control.	19
2.10	Double Stroke Threshold Stiffness Control.	20
3.1	In-plane model in Simulink.	23
3.2	Lengths of motorcycle.	25
3.3	Angles of motorcycle.	26
3.4	Original damping maps.	28

3.5	Relationship between the stroke and wheel jounce	29
3.6	Relationship between the stroke and swing arm angle (θ_s)	29
3.7	Compare road profile generation: amplitude-space relationship . .	31
3.8	Compare road profile generation: PSD	32
3.9	Road generation by using a transfer function method.	32
3.10	Multichamber dual chamber schematic.	33
3.11	RMS Cost function.	35
4.1	Front sensitivity KC.	37
4.2	Contact forces on tyres during front sensitivity.	37
4.3	Front stiffness sensitivity for accelerations with 100% damping. .	38
4.4	Front stiffness sensitivity for stroke variables with 100% damping.	38
4.5	Front stiffness sensitivity for accelerations with 20% damping. .	39
4.6	Front stiffness sensitivity for stroke variables with 20% damping. .	39
4.7	Front sensitivity J az.	40
4.8	Front sensitivity J ry.	40
4.9	Relative vertical acceleration-front	41
4.10	Relative pitch acceleration-front	41
4.11	Rear sensitivity KC.	42
4.12	Contact forces on tyres during rear sensitivity.	42
4.13	Rear sensitivity J az.	43
4.14	Rear sensitivity J ry.	43
4.15	Rear J az stiffness sensitivity range with different dampings. . .	44
4.16	Rear J ry stiffness sensitivity range with different dampings. . .	45
4.17	Contact forces on tyres during braking maneuver.	45
5.1	Multichamber suspension dimensions.	48
5.2	Tri-sensitivity for multichamber sizing	50
5.3	k_{low} and V_{aux} relationship	51
5.4	Ohlins SP36PL	52

LIST OF FIGURESxi

5.5	Ohlins MTB TTX2	53
6.1	Brute-force optimization algorithm	55
6.2	Selection of optimal stiffness	55
6.3	Shifting the optimization horizon	56
6.4	Brute-force optimization result compared with passive	57
6.5	Relative change in optimal comfort with respect to passive soft . .	58
6.6	Relative change in optimal comfort with respect to passive normal .	59
6.7	Vertical and pitch acceleration contribution in improving the over-all cost function	61

List of Tables

1.1	Multichamber final sized parameters	10
3.1	Rider inertial parameters	23
3.2	Motorcycle inertial parameters	24
3.3	Motorcycle Lengths	25
3.4	Motorcycle angles	26
3.5	Motorcycle stiffness parameters	27
3.6	Motorcycle preload parameters	27
3.7	Stiffness states using valve switch	34
5.1	Stiffness configurations for multichamber suspension	50
5.2	Multichamber sized parameters	51

Abstract

The comfort of a motorcyclist is one of the most important aspects for the journey. The motorcycle dynamics are excited causing discomfort to the rider due to the roughness in the road. Often thanks to semi-active suspensions damping control is used to improve the comfort. Recently, a different suspension technology called multichamber suspension has emerged in top end automotive vehicles due to their energy efficient technology to control of the suspension equivalent spring force. The control of the elastic force to improve the comfort is a new topic that is less explored both in the scientific literature and in industrial applications. The potential, in terms of comfort improvement, of this suspension technology is investigated in this thesis. In particular, its application to the rear suspension of a motorcycle, using a realistic vehicle model, is studied. Firstly, the passive stiffness sensitivity is carried out in order to understand the stiffness and damping configurations that allow improvement in comfort. Then a multichamber suspension is sized for these corresponding stiffness configurations. Finally, the brute-force optimization algorithm is performed to assess the capability of improvement of comfort using such a controllable stiffness technology. The thesis is a collaboration between Politecnico di Milano and Ducati, an internationally reputable company for high performance motorcycles.

Keywords: air spring, stiffness, suspension, comfort, vertical dynamics, pitch dynamics, motorcycle

Sommario

Il comfort di un motociclista è uno degli aspetti più importanti per il viaggio. La dinamica della moto viene continuamente stressata, provocando disagio al motociclista, a causa delle asperità della strada. Grazie alle sospensioni semi-attive, il controllo dello smorzamento è utilizzato per migliorare il comfort del motociclista. Recentemente, una diversa tecnologia di sospensione, chiamata sospensione multicamera, è emersa nelle automobili di fascia alta, grazie alla loro tecnologia ad alta efficienza energetica per il controllo della forza della molla equivalente alla sospensione. Il controllo della forza elastica per migliorare il comfort è un argomento nuovo e meno esplorato sia nella letteratura scientifica sia nelle applicazioni industriali. In questa tesi vengono indagate le potenzialità, in termini di miglioramento del comfort, di questa tecnologia di sospensione. In particolare, viene studiata la sua applicazione alla sospensione posteriore di una motocicletta, utilizzando un modello di veicolo realistico. In primo luogo, la sensibilità alla rigidità passiva viene effettuata al fine di comprendere le configurazioni di rigidità e smorzamento che consentono un miglioramento del comfort. Quindi una sospensione multicamera viene dimensionata per queste configurazioni di rigidità corrispondenti. Infine, un algoritmo brute-force di ottimizzazione viene eseguito per valutare la capacità di miglioramento del comfort, utilizzando così una tecnologia di rigidità controllabile. La tesi è una collaborazione tra il Politecnico di Milano e Ducati, azienda di fama internazionale per motociclette ad alte prestazioni.

Parole chiave: molla ad aria, rigidità, sospensioni, comfort, dinamica verticale, dinamica di beccheggio, motocicletta

Chapter 1

Introduction

Suspensions play a crucial role in the performance and comfort for any vehicle. The classical suspension consists of a stiffness and damping element that connects the wheel to the vehicle chassis. The semi-active suspensions consists of a variable damping element which is abundantly found in the scientific literature and industrial applications. By modulating the damping, the driving characteristics such as comfort and/or performance can be significantly improved as compared to a passive case. An active suspension on the other hand would modify the suspension force by injecting energy into the system. The capabilities of such suspensions are many but it suffers from a big disadvantage of high energy consumption.

Further research in electronically controllable suspensions has led to the development of variable stiffness technologies like the multichamber air-spring. A cross sectional view of such a real multichamber suspension used by Porche is shown in figure (1.1).

The multichamber suspension is an air-spring with auxiliary chambers and corresponding valves. The stiffness of this suspension is inversely proportional to the volume. Figure (1.2) shows the corresponding schematic highlighting the valves and the chambers of the suspension.



Figure 1.1: Cross-sectional view of a real Porsche multichamber suspension.

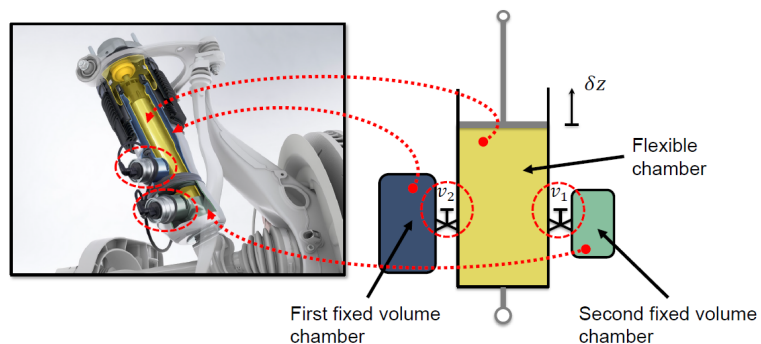


Figure 1.2: Sketch view of the Porche multichamber suspension.

The electronic valves allow for the total volume variation, as they connect/isolate the additional volume chambers. Considering all the possible valves configurations, a total number of 4 different volumes, hence suspension stiffness, can be achieved. The valves can be switched for fast switching of the suspension stiffness. The added advantage of multichamber suspensions over the active suspensions is their low power consumption capability as power is consumed only by the electronic actuators that modulate the chamber valves.

This thesis deals with the study and analysis of multichamber suspensions, in view of better understanding their potentials and advantages in ride comfort improvement.

1.1 Scope of Interest

In this thesis, a 2 state stiffness air-spring is considered for comfort capability analysis. The primary goal is to verify the potential benefits of a multichamber suspension, hence a brute force optimization is performed that serves as a benchmark.

The Quarter car vertical dynamics has already been covered in the past with the resulting conclusion of softer springs giving an improved comfort over the stiffer springs. Instead, the half car vehicle dynamics is studied in this thesis. In particular a motorcycle case study is analyzed where a detailed model of the vertical and pitching dynamics is covered. Due to the nature of half car dynamics, the vertical and pitch accelerations are needed to be taken into account to create the appropriate comfort cost function.

In summary, the thesis focuses on the possible comfort improvements that can be achieved by actively switching the stiffness using the rear suspension only (due to technological reasons) keeping the problem complexity reasonable but still in a realistic framework of motorcycles.

The control algorithm and mathematical models described in this work have

been realized in the MATLAB Simulink environment along with an in-plane dynamical multibody motorcycle simulator.

1.2 Main Contribution

The innovative contributions of this work are represented by the performing the passive sensitivity simulations in order to analyze the suitable location of multichamber suspension. Also, the effect of damping was investigated to fully understand the capability of improving comfort in a variable stiffness architecture. The multichamber suspension sizing is developed for motorcycle dimensions. A brute force optimization algorithm is implemented on a full vehicle (motorcycle) simulator as well.

1.2.1 Passive suspension design and analysis

The J_{az} cost function is computed by taking the rms (root mean square) of the vertical acceleration thereby quantifying towards the comfort due to vertical dynamics. The full range of change in cost function J_{az} is expressed by figures 1.3 and 1.4 for the rear and front suspensions respectively. The figures depict the span of comfort as a function of scaling factor on the damping. Both figures exhibit that the nominal damping gives a low span, thereby lower allowability in significant improvement of J_{az} comfort with a variable stiffness. Furthermore, the figures show that the low damping in rear has a much bigger range than the front so using the multichamber suspension on the rear with lower damping will allow us to explore the capability of multichamber suspension.

1.2.2 Multichamber sizing

The sizing of a motorcycle suspension is particularly crucial due to the smaller vehicle dimensions. A feasibility study was carried out in this thesis to have a

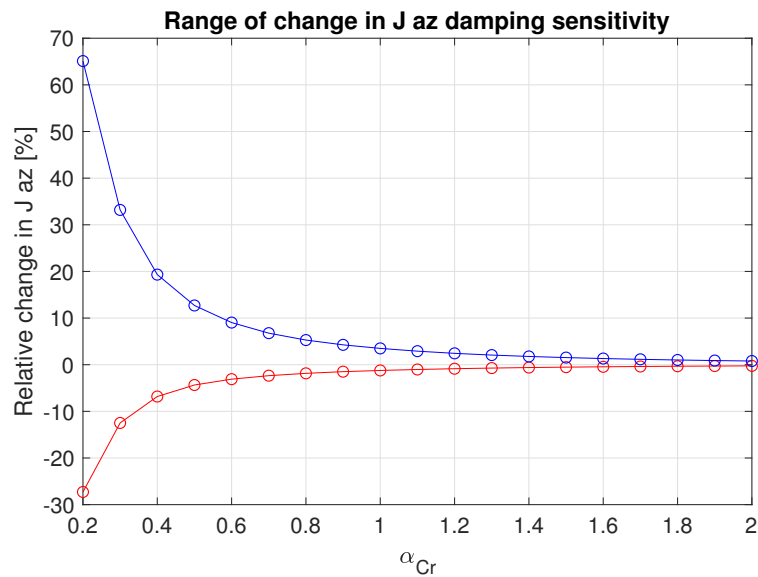


Figure 1.3: Rear suspension sensitivity with vertical cost function.

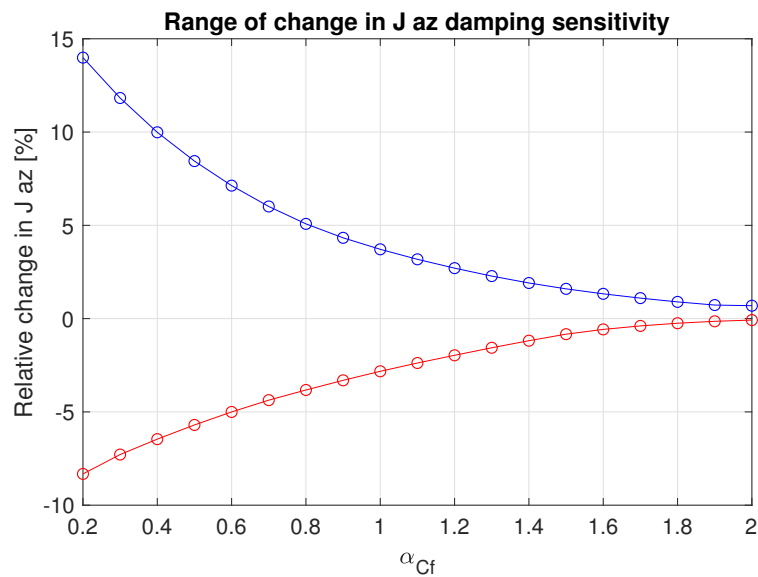


Figure 1.4: Front suspension sensitivity with vertical cost function.

multichamber suspension on the rear suspension of a motorcycle which was not formally investigated in any previous studies. The result is that the suspension is feasible with a reasonable sizing. The multichamber sizing was performed for a total of 7 suspensions. Table 1.1 shows the common multichamber parameters of the 7 suspensions with varying auxiliary chamber (V_{aux}) sizes from 17 mL to 1.5 L . The dimensions are marked in figure 1.5.

Parameter	Value	Units
Nominal pressure, p_0	7.84	bar
Radius, r	40	mm
Height, h	59.6	mm

Table 1.1: Multichamber final sized parameters

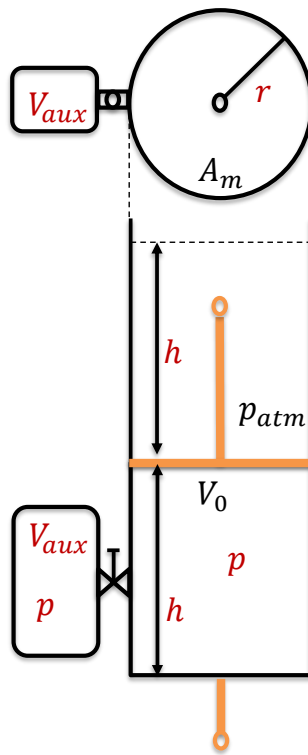


Figure 1.5: Multichamber suspension dimensions.

1.2.3 Optimization result

Using the optimization algorithm that will be described in this thesis later on, I have optimized the cost function (J_{tot}) that includes both pitch and vertical accelerations using a multichamber suspension with 2 chambers (i.e. one switching valve). Consequently, the optimization brought an interesting result because the comfort has improved with respect to the passive suspension. Figure (1.6) shows the relative change in cost function using the optimization algorithm with respect to the passive suspension as a function of the span of the 2 stiffness used for optimization. From passive analysis it was concluded that a larger span of change in J_{tot} is proportional to the span of stiffness, but with optimization it is noticed that a larger span does not give rise to more improvement in comfort as compared to the passive. A span of stiffness which is in between the largest and lowest value gives the maximum control benefit as shown in figure (1.6).

This confirms a similar trend in 2 state damping control algorithm for semi-active suspensions where the best performance is not obtained when the span between the damping is big.

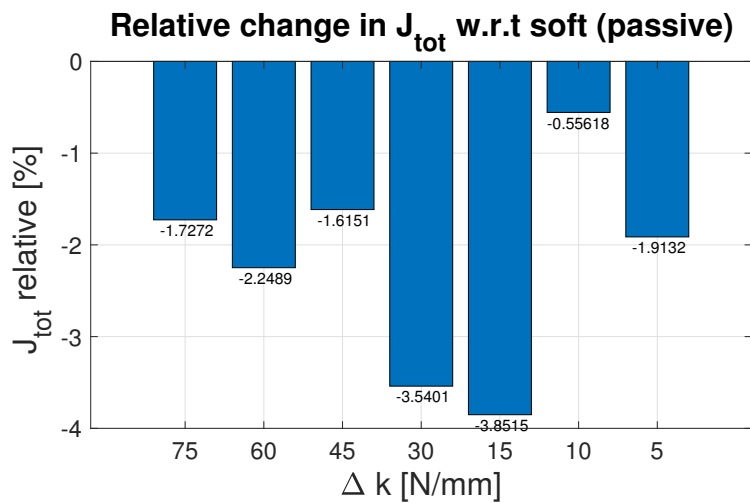


Figure 1.6: 2 state optimization sensitivity using J_{tot} cost function.

1.3 Structure of the Thesis

The thesis is organized as follows:

Chapter 2 shows the current technological and algorithmic state of the art for variable stiffness suspensions used in vehicles. Different technologies are mentioned which can modify the suspension stiffness and existing control algorithms that can modulate the elastic force in literature.

Chapter 3 explains the mathematical model of the multichamber suspension, development of the comfort cost function and motorcycle simulation parameters. It also explains the usage of lever ratio and the road profile generation technique employed for the analysis.

Chapter 4 presents the passive stiffness sensitivity result using a passive spring and passive damper. After the analysis, it is concluded that a nominal damping of motorcycle is not sufficient to perform the optimization of stiffness to improve comfort.

Chapter 5 strategizes the sizing steps carried out to realize a practical suspension. The different parameters of the suspension such as area of piston, height of suspension, pressure need to be appropriately selected to physically fit in the motorcycle and be realised practically.

Chapter 6 implements the optimization routine to assess the comfort improvement. The working of brute-force optimization algorithm is discussed. The contribution of pitch and vertical acceleration towards the total cost function improvement is also discussed in this section.

Chapter 7- Conclusions contains the brief summary of all the main results derived from this work.

Chapter 2

State of art

A brief discussion of the different suspensions are discussed in this chapter that have the capability to vary stiffness. In the end of these technologies, the multichamber suspension is chosen for the optimization algorithm. The different algorithms that implement a variable stiffness control strategy are also discussed which either focus on the performance or the comfort characteristic.

2.1 Variable stiffness technologies

2.1.1 Horizontal strut based passive variable stiffness

The passive variable stiffness technology by Patel et al. [6]), is a method of varying the stiffness using the mechanical structure arrangement. The realistic model of such an arrangement is shown in Figure 2.1. In the schematic version (Figure 2.2), it is seen that the displacement of top block (m_d) will give rise to the variability of the stiffness due to the displacement of spring-damper system. The performance of the constant stiffness (by blocking m_d) and passive variable stiffness (freely moving m_d) is compared, where the passive outperforms the constant in terms of comfort, road contact and suspension deflection. Even though it does better than a constant stiffness, the drawback is that we cannot implement a control

strategy to modulate the stiffness of this suspension.



Figure 2.1: Strut based Passive variable stiffness technology.

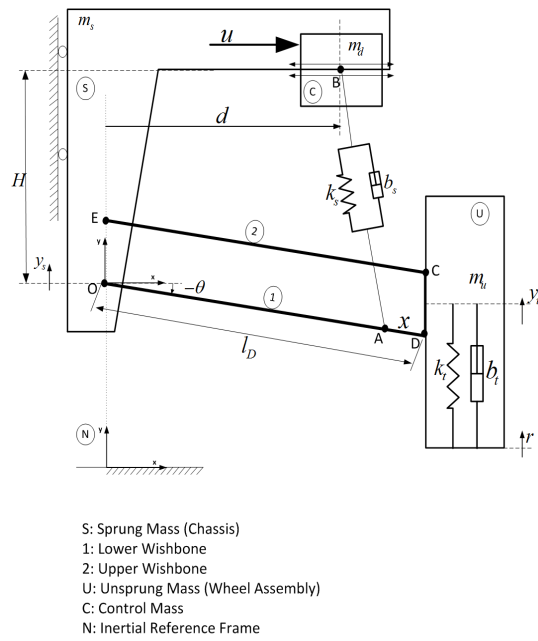


Figure 2.2: Strut based Passive variable stiffness technology (schematic).

2.1.2 Magnetic suspension system

A magnetic based ([8]) suspension is proposed which has been used for space instruments and carrier systems in clean rooms. The main components of this suspension (figure 2.3) are the floater element connected to a permanent magnet, a current source and an electromagnet. The electromagnetic field can be varied by modifying the current value. The stiffness-current is given by the map in figure 2.4. Theoretically, such a stiffness has the capability to have infinite stiffness. Additionally, it has the ability to have negative and positive stiffnesses to have a wider range of stiffness operations.

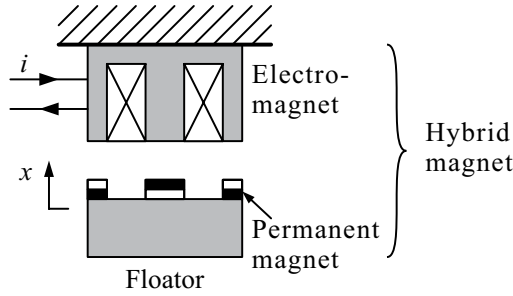


Figure 2.3: Schematic of magnetic suspension system.

2.1.3 Damper based variable stiffness

A variable stiffness technology is developed in [4] by the use of a controllable damper in series and parallel with a passive spring as shown in figure 2.5 . The controllable damper (from figure 2.6) is able to change the damping to 8 different values, by changing the number of active holes. The active holes determine a unique damping value as they change the viscosity characteristic of the damper.

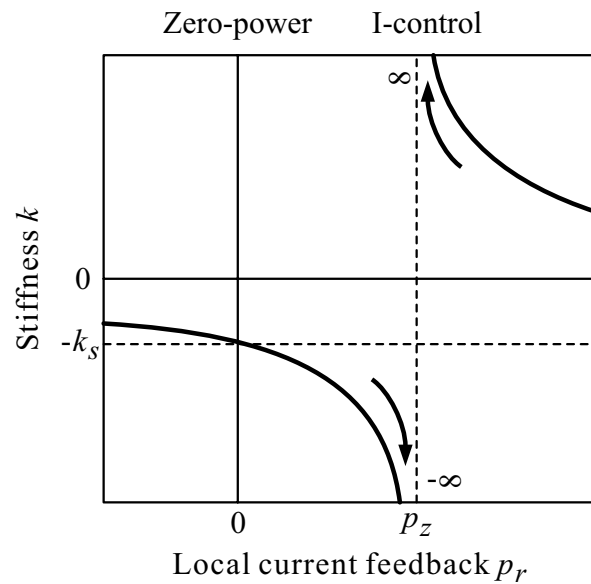


Figure 2.4: Stiffness vs current graph for magnetic suspension system.

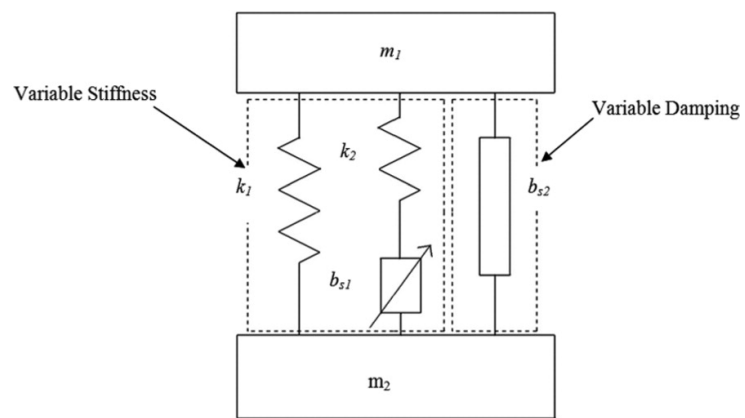


Figure 2.5: Variable stiffness based on modulating damper.

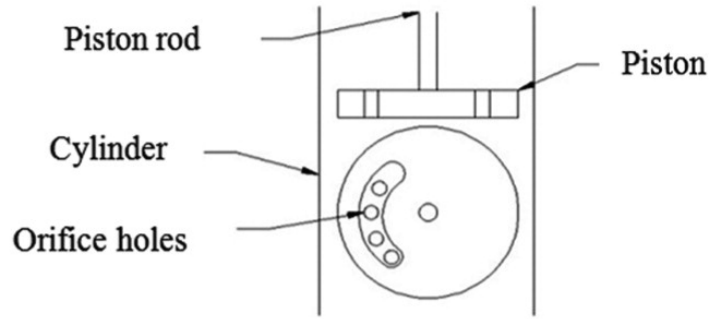


Figure 2.6: Variable damper.

2.1.4 MR (magnetorheological) elastomer isolator

The MR elastomer (MRE) isolator technology is used by Du et. al ([3]) for making a semi-active variable stiffness control of vehicle seat suspension. By changing the input current, the magnetic property can be modified thereby chaning the effect of suspension. Figure 2.7 shows the schematic of this technology. The current in the coil forms the electromagnet which will influence the MRE element and thereby effecting the stiffness. The dependence of current vs stiffness for the MRE is shown in Figure 2.8

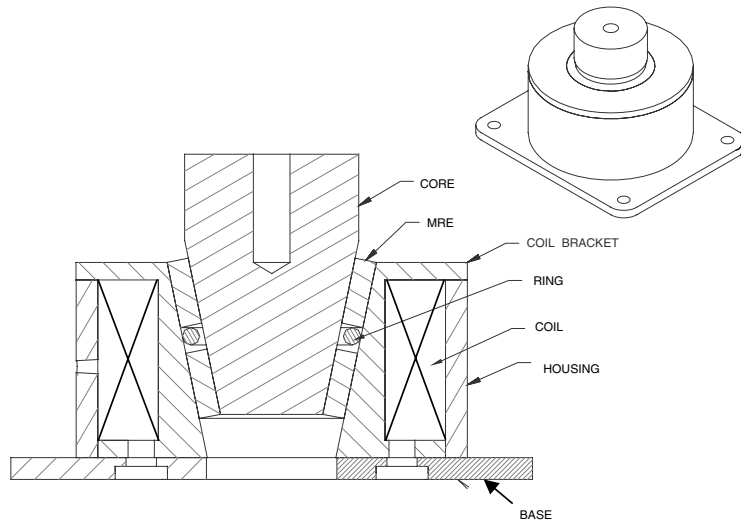


Figure 2.7: MRE schematic.

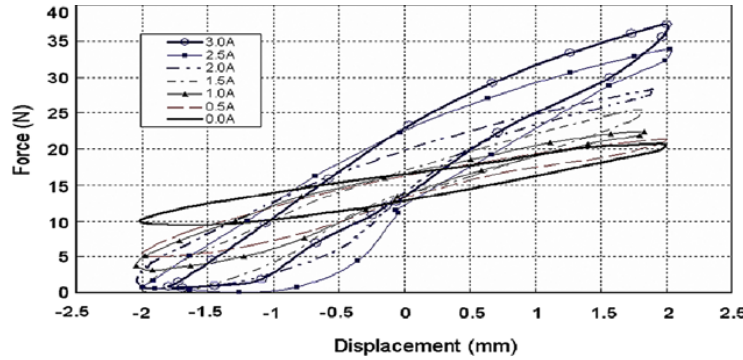


Figure 2.8: Current sensitivity for MRE technology.

2.1.5 Multichamber suspension

The multichamber suspension is the main variable stiffness suspension technology that is used in this topic. The advantages of this variable stiffness suspension over others is that it allows a fast switching of the stiffness by only actuating the valves. The switching mechanism consumes low power. Unlike other variable stiffness technologies, it only allows for 2-3 stiffness states (depending on the number of chambers). This suspension works on the principle of change volume that is inversely proportional to the stiffness. Additionally, the opening of the valves causes certain dynamics which gives rise to additional force spikes or kick forces. We would like to harness these kick forces to our advantage in order to improve the comfort as well. The multichamber suspension's dynamical model and architecture will be discussed in more detail in the subsequent modelling chapter.

2.2 Algorithms using Variable stiffness

2.2.1 Stroke Speed Threshold Stiffness Control (SSTSC)

This is a comfort based algorithm discussed in [7]. Soft springs give the best comfort at the expense of easy to hit the endstops. The main idea of this algorithm would be to keep the stiffness as soft when the stroke and stroke speed is low (away from the end stops or approaching the end stops lower) and increase the stiffness when the stroke and stroke speed is high (closer to the end stops or approaching the end stops faster). The damping uses a mix skyhook-add algorithm. The multichamber suspension would give rise to additional kick forces when the valves open (when the stiffness changes from hard to soft). Figure 2.9 shows such a switching pattern when the stroke and stroke rate states cross the thresholds and return from hard to soft configuration.

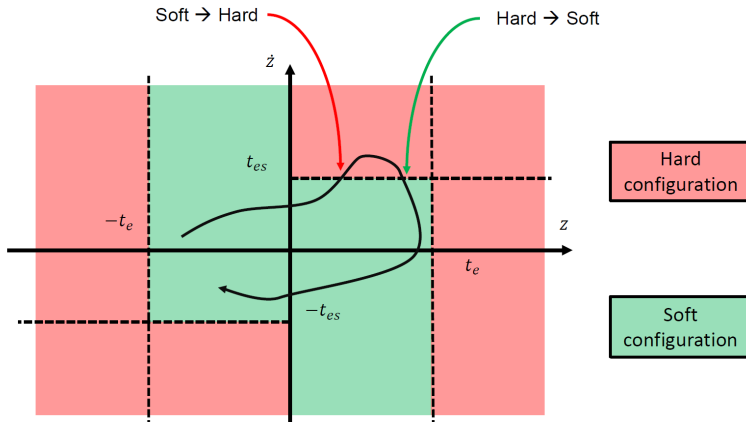


Figure 2.9: Stroke Speed Threshold Stiffness Control.

2.2.2 Double Stroke Threshold Stiffness Control (DSTSC)

Figure. 2.10 shows a more implementable scheme using the multichamber suspension in which only the stroke state is of concern to avoid hitting the endstops. This algorithm is a stepwise increment of the stiffness based on the position of

the stroke. The closer it reaches the end stop limit, the stiffer the spring becomes. The problem of unwanted kick forces using a multichamber suspension does not occur in this algorithm as the valves open and close at the same stroke travel.

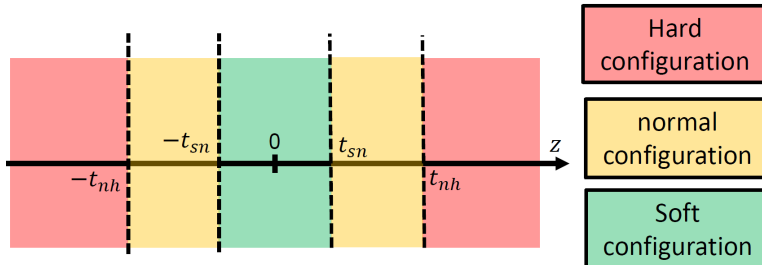


Figure 2.10: Double Stroke Threshold Stiffness Control.

2.2.3 Stiffness and damping control to reduce dynamical effects

This [[5]] paper discusses the control of stiffness and damping coefficients in order to reduce the dynamical effects for off road vehicle conditions. In particular the real time control strategy focuses to minimise the change in ground clearance of the vehicle. The transfer function is written with the position of axle as input and the position of suspended mass as output. Then the second order denominator is tuned in order to reduce the settling time. The final control algorithm obtained is given by 2.1.

$$\begin{aligned} k_{s,i} &= \frac{\pi^2}{A_i(t)t_{p,i}^2(1-\xi^2)} \\ c_{s,i} &= \frac{2\xi\pi}{A_i(t)t_{p,i}^2(1-\xi^2)} \end{aligned} \quad (2.1)$$

where $A_i(t)$ corresponds to load transfer coefficients, ξ is the damping ratio and $t_{p,i}$ is the peak time.

2.3 Conclusion

The comparison of the multichamber suspension over the other architectures shows its potential in being suitable for vehicle application by consuming low power and high switching frequency. Different variable stiffness algorithms are mentioned which attempt to deliver the potential of this multichamber suspension in real time vehicle suspension control strategies. In order to fully explore the potential benefits of this switching stiffness multichamber suspension, a brute-force optimization can serve as the benchmark.

Chapter 3

Simulation setup

3.1 Motorcycle simulator

The in-plane model simulator is a multibody dynamical motorcycle simulator. A snapshot of the simulink based simulator is shown in figure 3.1. It accounts for the longitudinal and vertical dynamics of the motorcycle. The inputs for the model are wheel torques, suspension forces (combination of spring and damper), road profile for both wheels front and rear. In order to start the simulation, an initial longitudinal velocity must be specified.

There are a lot of outputs measured using the in-plane model simulator such as vehicle speed, acceleration, tyre compression, position of COG etc. Suspension variables like stroke and stroke rates, suspension forces, accelerations (pitch and vertical) are particularly relevant to us as the topic deals with suspension control where pitching and vertical dynamics are of primary concern.

3.1.1 Masses and moment of inertias in the simulator

The simulator uses the inertial parameters of the motorcycle, given in table (3.2) and the inertial parameters of the rider, given in table (3.1).

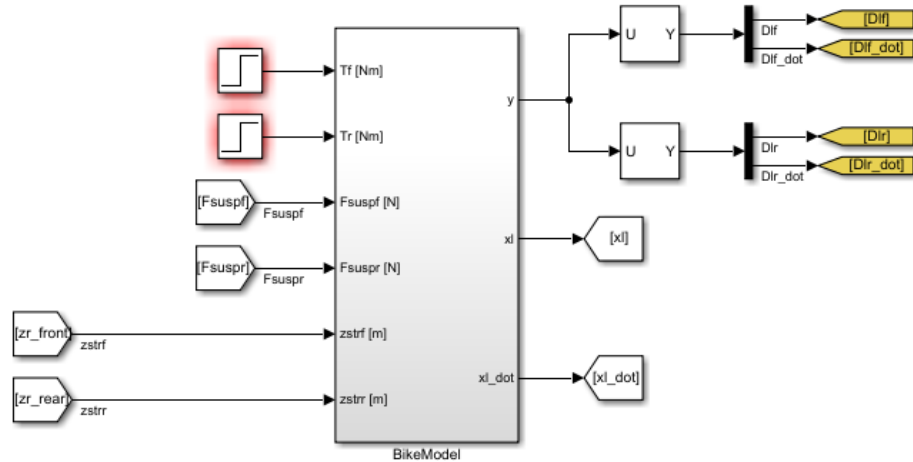


Figure 3.1: In-plane model in Simulink.

Parameter	Units	Value
Rider mass (upper)	kg	43.52
Rider mass (lower)	kg	25.84
Rider moment of inertia (upper)	$kg\ m^2$	1.347
Rider moment of inertia (lower)	$kg\ m^2$	0.5

Table 3.1: Rider inertial parameters

Parameter	Units	Value
Body sprung mass	kg	188.4
Front tyre mass	kg	11.8
Rear tyre mass	kg	18.2
Fork mass	kg	8.2
Handlebar mass	kg	9.99
Swing arm mass	kg	14.1
Body pitch moment of inertia	$kg\ m^2$	30.8
Front fork moment of inertia	$kg\ m^2$	1.584
Front wheel moment of inertia	$kg\ m^2$	0.52923
Rear wheel moment of inertia	$kg\ m^2$	0.91445

Table 3.2: Motorcycle inertial parameters

3.1.2 Dimensions of the motorcycle

The lengths and angles of the motorcycle are given by figure 3.2 and figure 3.3 respectively. The corresponding labels of the figures are explained in table (3.3) and table (3.4) respectively. In order to obtain the vertical speed of the seat position, a sensor is placed at the location whose position is defined by L_{sensor} (distance from the handlebar) and A_{sensor} (inclination from the handlebar horizontal line).

3.1.3 Stiffness and damping elements

The tyres stiffnesses and suspension stiffnesses are shown in table (3.5) while the preloads are given in table (3.6). The preloads have to be chosen such that the pitch and the suspensions stroke of the motorcycle are close to zero in a flat road profile. The suspension dampings are nonlinear functions, the damping force-stroke rate relationship is given by figure 3.4 for front and rear suspensions. The suspension force inputs are computed externally using the vehicle state measures



Figure 3.2: Lengths of motorcycle.

Parameter	Units	Value
L_f	mm	838
L_{sensor}	mm	680
L_{wb}	mm	1529.8
R_f	mm	317
R_r	mm	299.5
H_{sa}	mm	407.3
L_{sa}	mm	569.9
X_{COG}	mm	726.8
Z_{COG}	mm	639.6

Table 3.3: Motorcycle Lengths



Figure 3.3: Angles of motorcycle.

Parameter	Units	Value
A_{sensor}	deg	21
A_{caster}	deg	23.5

Table 3.4: Motorcycle angles

provided by the simulator.

Parameter	Units	Value
Tyre stiffness front	N/mm	175
Tyre stiffness rear	N/mm	165
Suspension stiffness front	N/mm	12
Suspension stiffness rear	N/mm	90

Table 3.5: Motorcycle stiffness parameters

Parameter	Units	Value
Preload front	N	3434.8
Preload rear	N	1266.7

Table 3.6: Motorcycle preload parameters

3.1.4 Rear wheel jounce and stroke relationship

For motorcycles, the lever ratio is the ratio of the suspension stroke to wheel jounce. Since it is not constant for the motorcycle considered, this relationship between the rear wheel jounce and rear suspension stroke is depicted in figure 3.5 and equivalently as the map between the rear swing arm angle and the rear suspension stroke in figure 3.6. The conversion between the wheel jounce to the rear swing arm angle is provided by the kinematic equation 3.1. As a matter of fact, the rear suspension lever ratio can be efficiently described by a linear relationship with equation 3.2.

$$\theta_s = A_{caster} - \sin^{-1}(\sin(A_{caster}) - \frac{(Jounce)}{L_{sa}}) \quad (3.1)$$

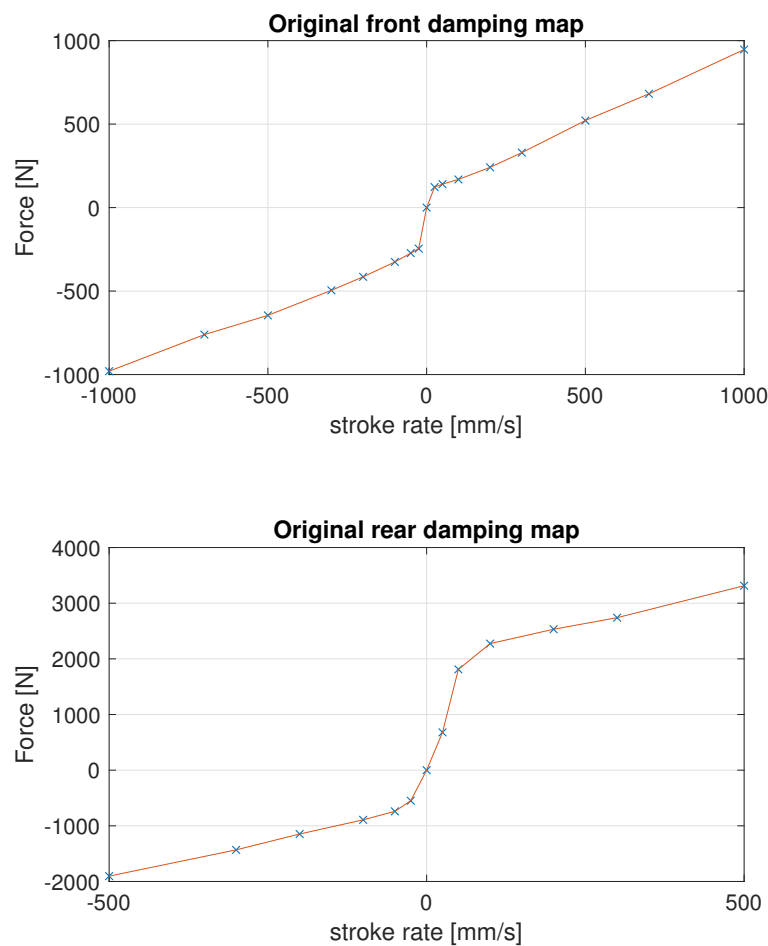


Figure 3.4: Original damping maps.

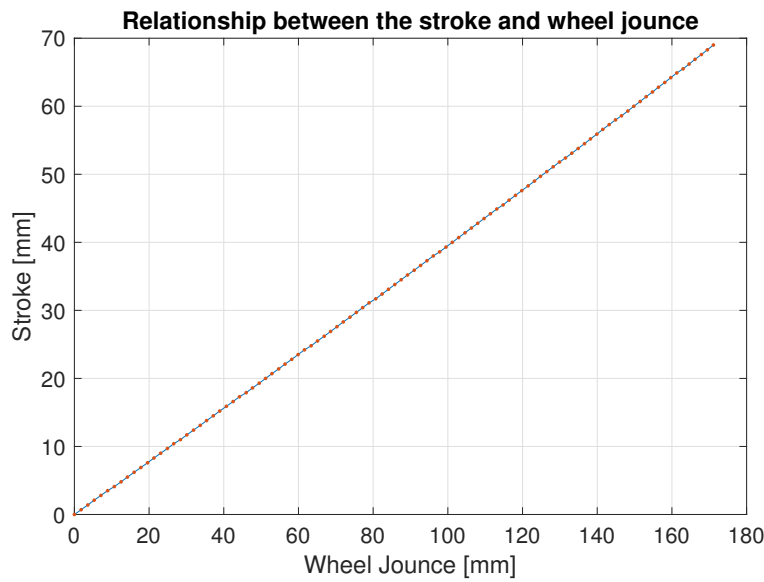


Figure 3.5: Relationship between the stroke and wheel jounce

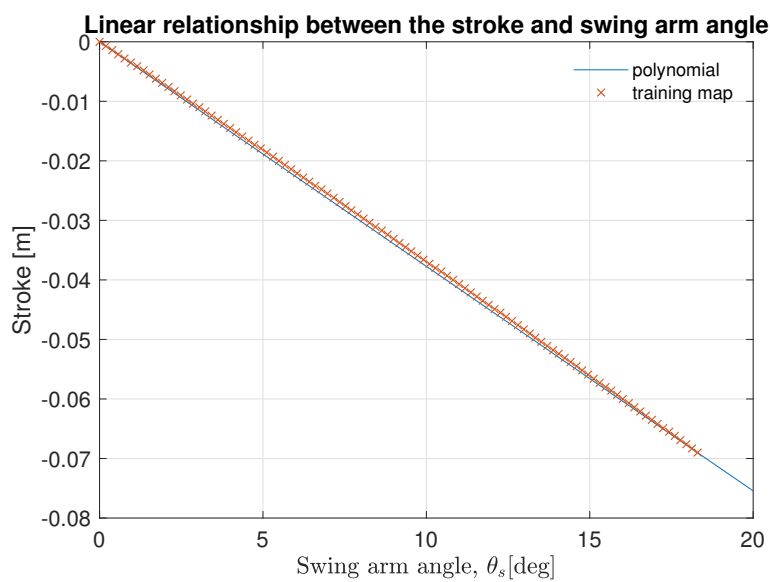


Figure 3.6: Relationship between the stroke and swing arm angle (θ_s)

$$\text{stroke} = -0.0038 * \theta_s \quad (3.2)$$

3.1.5 Derivative of sensor speed

The vertical acceleration of the sensor location (located at the seat) is of importance as it will be used to compute the comfort cost function. Since it is only possible to obtain the vertical speed and not acceleration, a derivative must be done. Passing the vertical speed signal through a derivative can lead to inaccurate and noisy signal so a filtered derivative is used as shown in equation (3.3), where ω_{sensor} is equal to the cutoff frequency of the filter. A reasonable cutoff frequency would be 100 Hz for practical purposes that is carried out throughout the analysis.

$$G_{derivatefilter}(s) = \frac{s}{(\frac{s}{2\pi\omega_{sensor}} + 1)^2} \quad (3.3)$$

3.1.6 Road profile

Road profile generation method by Agostinacchio

One method to create the road profile is the one suggested by Agostinacchio in [1] and given by equation (3.4).

$$z_r(x) = \sum_{i=0}^N \sqrt{\Delta n} 2^k 10^{-3} \left(\frac{n_0}{i \Delta n} \right) \cos(2\pi i \Delta n x + \varphi_i) \quad (3.4)$$

The drawback of road generation using this method is that it is computationally inefficient, especially for long road profiles. For a road profile of 1 km would take 1.4 seconds while 10 km would take 76 seconds. Another problem is that the longer the road profile is, the higher the low frequency component of the road appears (hill effect). The hill effect can be tackled by using multiple smaller road segments and stitch together to create a longer road profile but the

computational cost remains. Instead an alternative transfer function method to generate road profile is used.

Road profile generation using transfer function method

A unitary white noise is passed through a transfer function (from equation 3.5) as shown in figure 3.9. The transfer function parameters are $\omega_r = \frac{2\pi v}{l_c}$ and $\zeta_r = 0.7$. The forward speed of the vehicle is v and l_c is road profile length. The parameter k_r is determined by the road quality ($S_{z_r}(\Omega_0)$) related by equation 3.6. The upper bound for $S_{z_r}(\Omega_0) = 2 * 10^{-6} m^3/rad$ for a class A road profile.

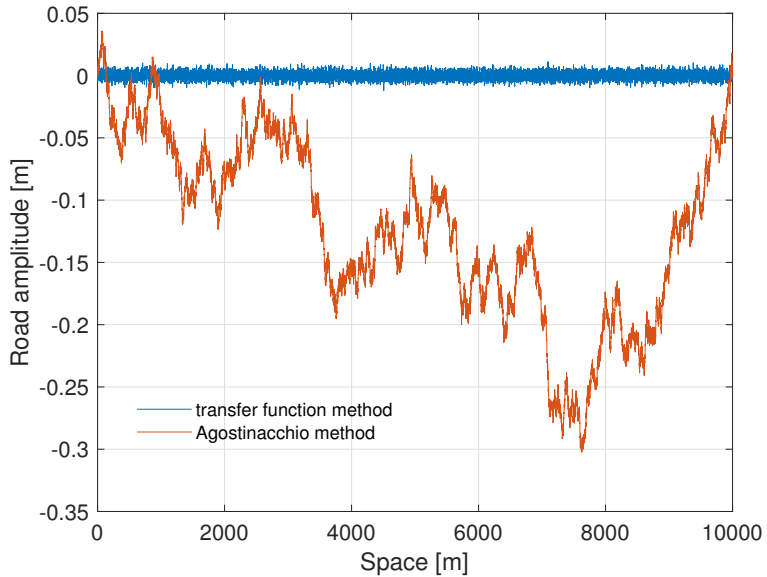


Figure 3.7: Compare road profile generation: amplitude-space relationship

The road amplitude-space map by both generation methods are shown in 3.7 for class A road profile. The Agostinacchio method clearly has a more hilly effect. This is further seen in the spectrum of the road amplitude signals from both methods in figure 3.8 where the transfer function method's road spectrum is spread out over the frequencies while the Agostinacchio's road has stronger low frequency components.

The transfer function method solves both the hill effect and long computa-

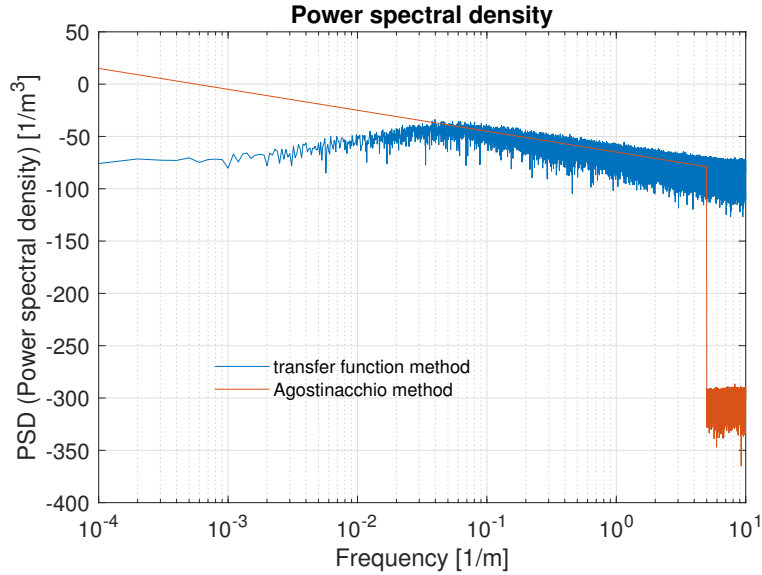


Figure 3.8: Compare road profile generation: PSD

tional time problems. The computational time to generate 1 km or 10 km will be less than 1 second. Class A road profile generated using the transfer function method is used by the simulator in subsequent chapters.

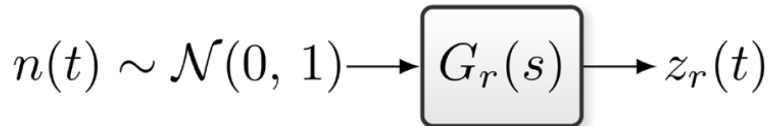


Figure 3.9: Road generation by using a transfer function method.

$$G_r(s) = \frac{k_r s}{s^2 + 2\zeta_r \omega_r s + \omega_r^2} \quad (3.5)$$

$$k_r = v \sqrt{\frac{S_{z_r}(\Omega_0)}{v}} \quad (3.6)$$

3.2 Multichamber suspension model

The multichamber suspension is the primary object of interest in this topic. The model used to integrate in the simulation is explained in this subsection which

is taken from [2]. The multichamber schematic model is depicted in figure 3.10. The main chamber is a cylinder with pressurized air filled in it. The cylinder has a movable piston head. The rings on the piston head and base of the cylinder are connected to the wheel and chassis in parallel to the damping element. As the stroke between the wheel and chassis changes due to ride dynamics, the suspension's piston head consequently moves as well causing a change in volume. The auxiliary chamber is connected parallelly to the main chamber through a single state valve. The state of the valve is given by $s(t)$ and described by equation 3.8.

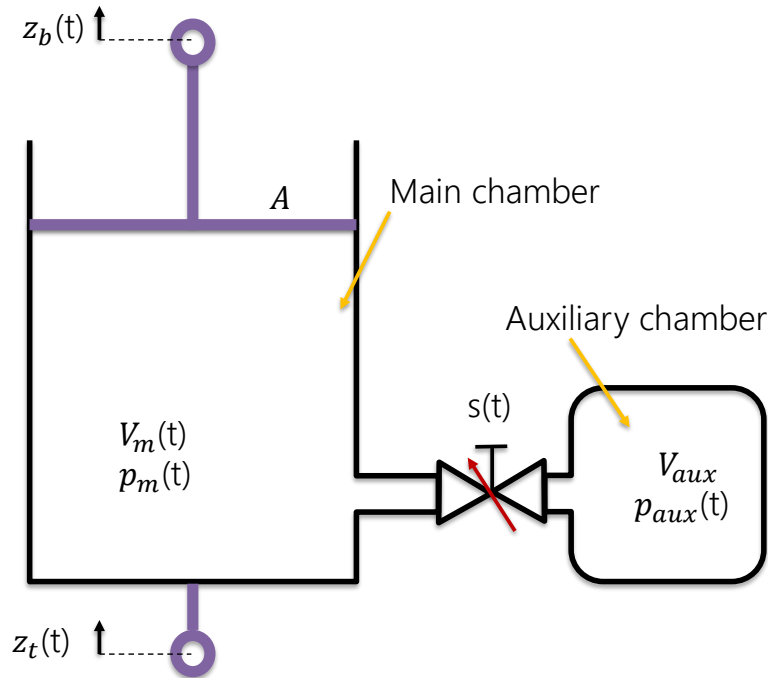


Figure 3.10: Multichamber dual chamber schematic.

$$k = \frac{pnA^2}{V} \quad (3.7)$$

Table 3.7 shows the effect of switch $s(t)$. It determines the stiffness of the suspension as the stiffness is inversely proportional to the volume according to equation 3.7.

Stiffness value	Valve state
High	Close
Low	Open

Table 3.7: Stiffness states using valve switch

$$s(t) = \begin{cases} 1 & (\text{valve opened}) \\ 0 & (\text{valve closed}) \end{cases} \quad (3.8)$$

The differential equations used to compute the pressure states of the 2 chambers are given by equation 3.9. Whenever the valves switch from closed to open state, then the initial conditions of the differential equations needs to be recomputed and initialised accordingly which is shown by equation 3.11. The initial conditions which are the equilibrium values, is computed according to the equation 3.10.

$$\begin{aligned} \dot{p}_m(t) &= -\frac{np_m(t)A(\dot{z}_b - \dot{z}_t)}{V_m(t) + s(t)V_{aux}} \\ \dot{p}_{aux}(t) &= -\frac{np_{aux}(t)A(\dot{z}_b - \dot{z}_t)}{V_m(t) + V_{aux}}s(t) \end{aligned} \quad (3.9)$$

$$p^{eq}(t) = \frac{p_m(t)V_m(t) + p_{aux}(t)V_{aux}}{V_m(t) + V_{aux}} \quad (3.10)$$

$$\begin{aligned} \text{if } s(\bar{t}^-) = 0 \wedge s(\bar{t}^+) = 1 \longrightarrow & \begin{cases} p_{m0} = p^{eq}(\bar{t}^-) \\ p_{aux0} = p^{eq}(\bar{t}^-) \end{cases} \\ \text{if } s(\bar{t}^-) = 1 \wedge s(\bar{t}^+) = 0 \longrightarrow & \begin{cases} p_{m0} = p(\bar{t}^-) \\ p_{aux0} = p(\bar{t}^-) \end{cases} \end{aligned} \quad (3.11)$$

The assumption of this mathematical model is that instantaneous equilibrium is reached upon opening of the valves. The optimization will still be representative of a real vehicle as the refresh time of stiffness will be much longer than the typical settling time of reaching equilibrium states.

3.3 Comfort cost function

The comfort cost function is given by the representation in figure 3.11. The vertical sensor and pitch accelerations rms value is taken, then squared (A^2 block) and weighted and added to obtain the total comfort cost function value (J_{tot}). The J_{az} and J_{ry} are the vertical and pitch cost functions respectively. The magnitudes of the vertical and pitch cost functions are starkly different, so it needs to be normalised (using the weights $W_{vertical\ acc}$ and $W_{pitch\ acc}$). The value of the normalizing weights will be discussed at the end of Chapter 4.

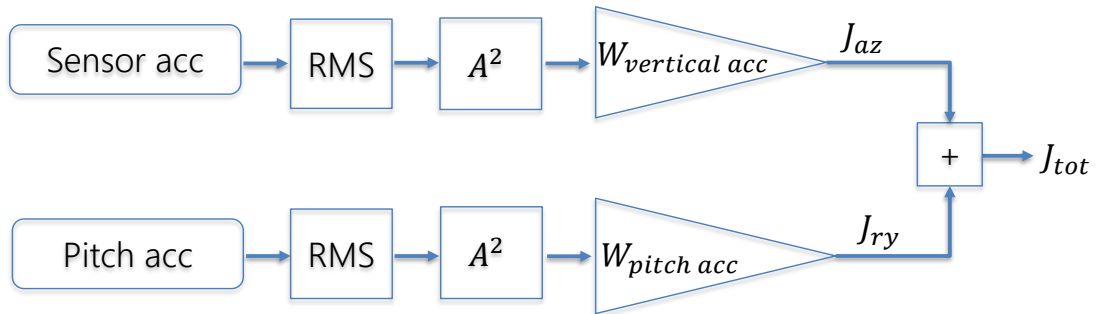


Figure 3.11: RMS Cost function.

Chapter 4

Passive sensitivity analysis

In this chapter, the passive stiffness and damping sensitivity of the motorcycle is presented. The motorcycle is simulated with a class A road profile at a speed of 90 kmph for 100 seconds.

The sensitivity analysis is first carried out for the front suspension and then for the rear suspension. After the analysis, it is seen that the nominal damping of the motorcycle is too high to have any considerable effect of improvement in comfort by the stiffness. The results of the front and rear are compared and it will be decided that the rear suspension is suitable for the multichamber optimization at a lowered damping to investigate the benefit of comfort. Finally the longitudinal dynamics are also investigated in order check the reasonability of reducing damping.

4.1 Front suspension sensitivity

The front stiffness is relatively softer (12 N/mm) than the rear spring (90 N/mm). The front damping map has already been shown in the previous chapter in fig 3.4. Only the front stiffness and damping scaling factors are varied as shown in figure 4.1 where the α_{kf} and α_{cf} vary from 0.2 to 2. The motorcycle contact

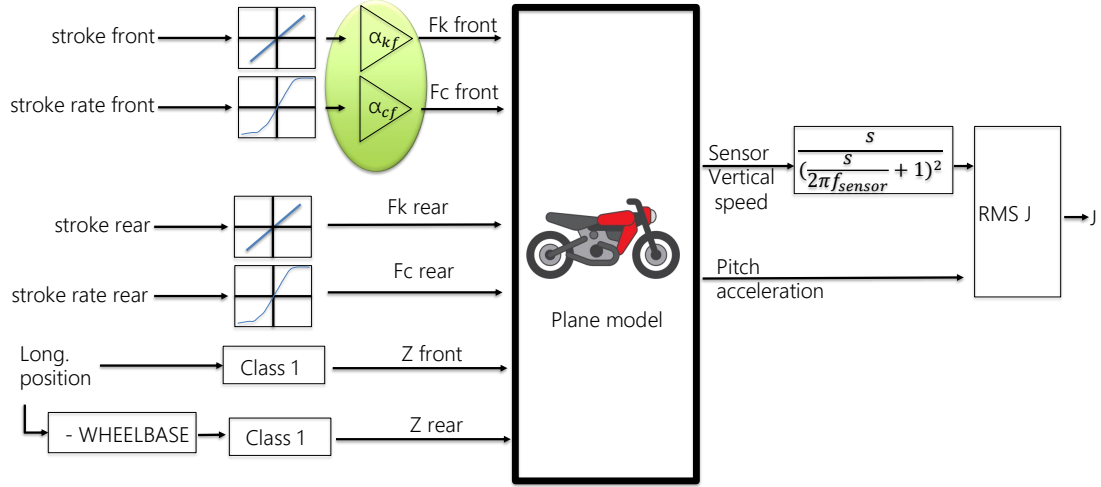


Figure 4.1: Front sensitivity KC.

forces are checked to make sure they don't go to 0 so that motorcycle has not lost road contact as shown in figure 4.2. A time-domain plot shows the stiffness

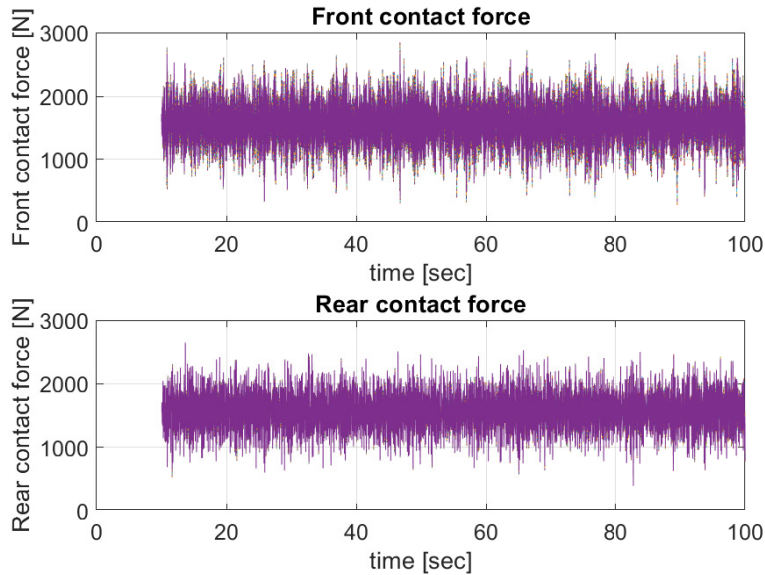


Figure 4.2: Contact forces on tyres during front sensitivity.

sensitivity at nominal damping in figure 4.3 and 4.4 for comfort accelerations and suspension stroke variables. The change in the acceleration is negligible whether a stiff spring is used or a soft whereas the stroke is affected.

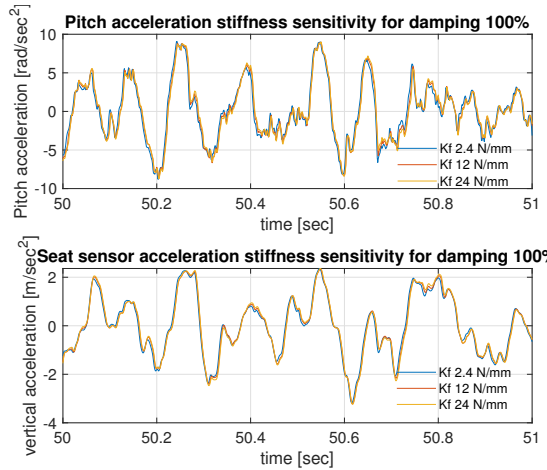


Figure 4.3: Front stiffness sensitivity for accelerations with 100% damping.

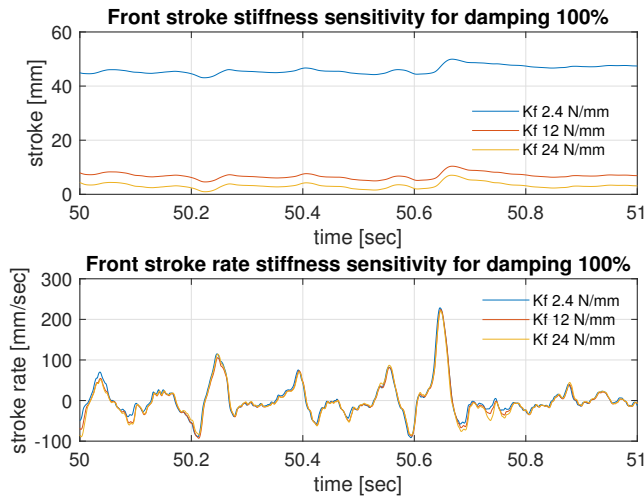


Figure 4.4: Front stiffness sensitivity for stroke variables with 100% damping.

Then the stiffness sensitivity is checked at the low damping (20% or $\alpha_{cf} = 0.2$) in figure 4.5 and 4.5. In low damping there is much more change in the accelerations when the stiffness is changed. The softer spring produces a higher stroke thereby coming close to the endstops whereas the acceleration is reduced much more.

The RMS of accelerations (pitch and vertical) is computed for all combinations of α_{cf} and α_{kf} and a 3d curve is plotted as shown in figure 4.7 for seat sensor

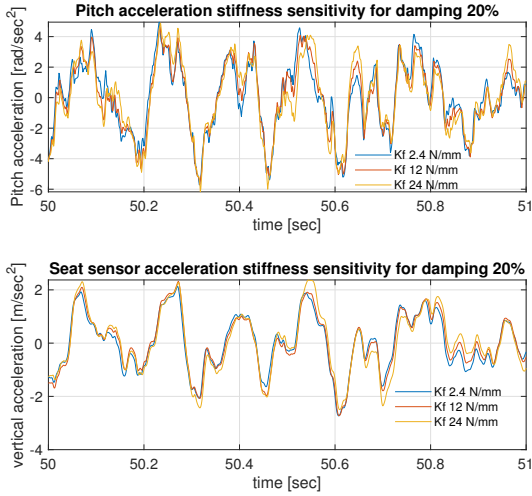


Figure 4.5: Front stiffness sensitivity for accelerations with 20% damping.

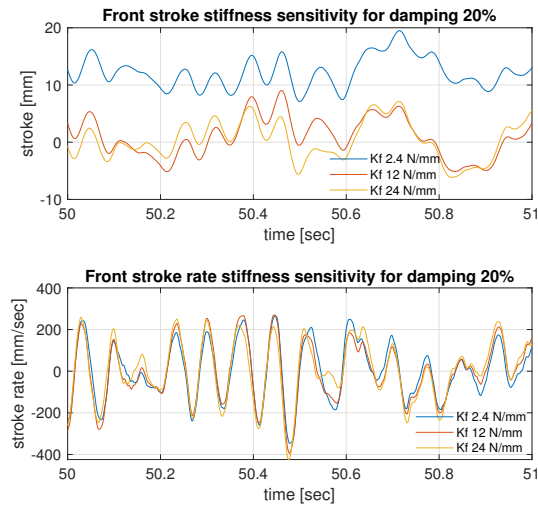


Figure 4.6: Front stiffness sensitivity for stroke variables with 20% damping.

vertical acceleration and 4.8 for pitch acceleration. It is seen that at higher dampings the effect of change in both cost functions is reduced.

Figure 4.9 and 4.10 shows the maximum (blue) and minimum (red) change in the cost functions as compared to the nominal stiffness as a function of damping scaling factor for vertical (J_{az}) and pitch (J_{ry}) cost functions respectively.

The peculiarity in the pitch sensitivity range is that around nominal damping

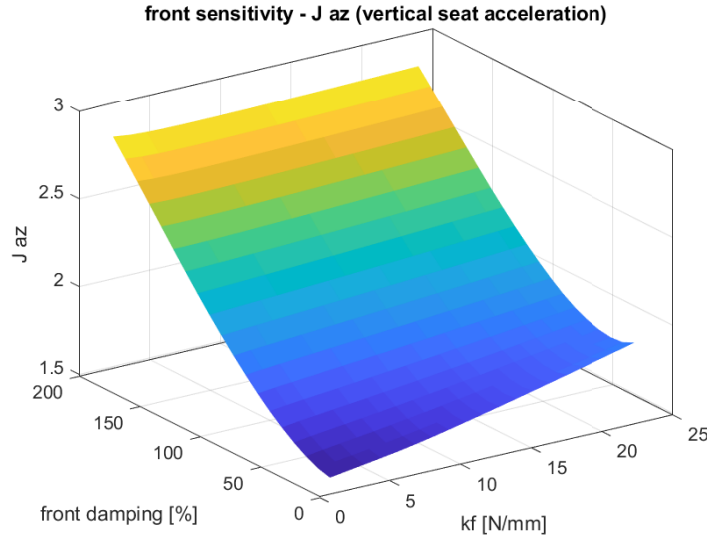


Figure 4.7: Front sensitivity J_{az} .

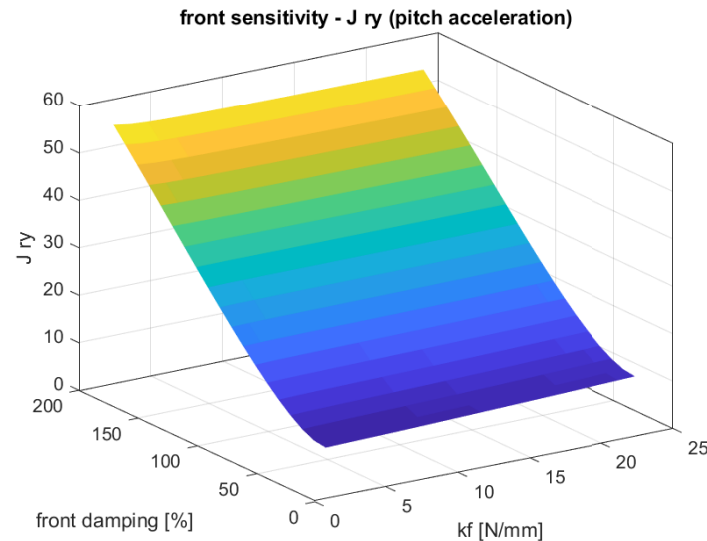


Figure 4.8: Front sensitivity J_{ry} .

where $\alpha_{cf} = 1$, the relative pitch acceleration performance range is the least. The relative vertical acceleration performance range on the other hand decreases with increasing damping, as the damping force value increases and negates any modulation of the spring force.

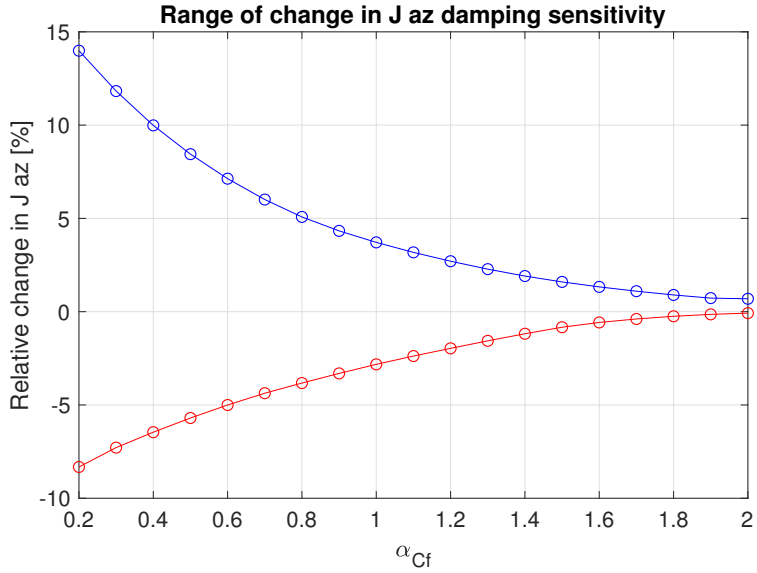


Figure 4.9: Relative vertical acceleration-front

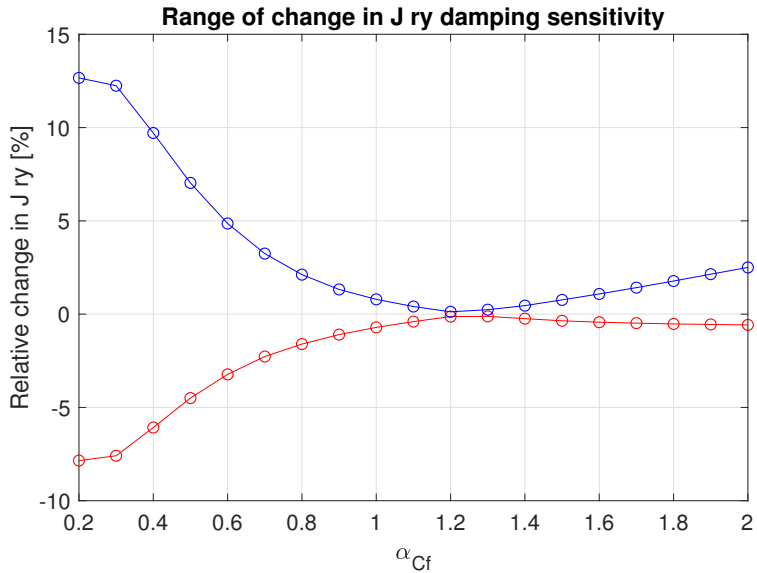


Figure 4.10: Relative pitch acceleration-front

4.2 Rear suspension sensitivity

The front stiffness and damping scaling factors are varied as shown in figure 4.11 where the α_{kr} and α_{cr} vary from 0.2 to 2. Similar to the front sensitivity, the front stiffness and damping is kept as it is original and only the rear suspension

is modified.

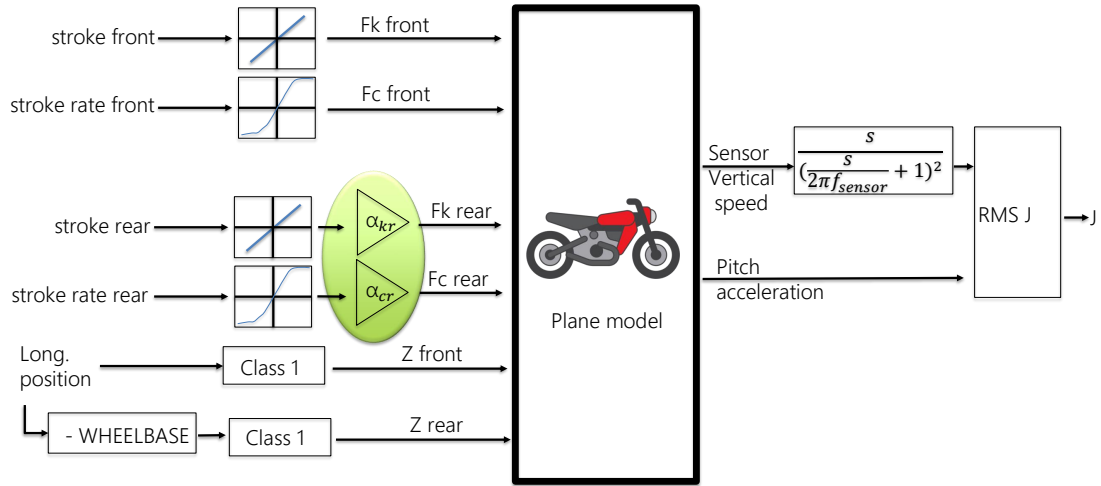


Figure 4.11: Rear sensitivity KC.

The motorcycle contact forces are checked to make sure they don't go to 0 so that motorcycle has not lost road contact as shown in figure 4.12.

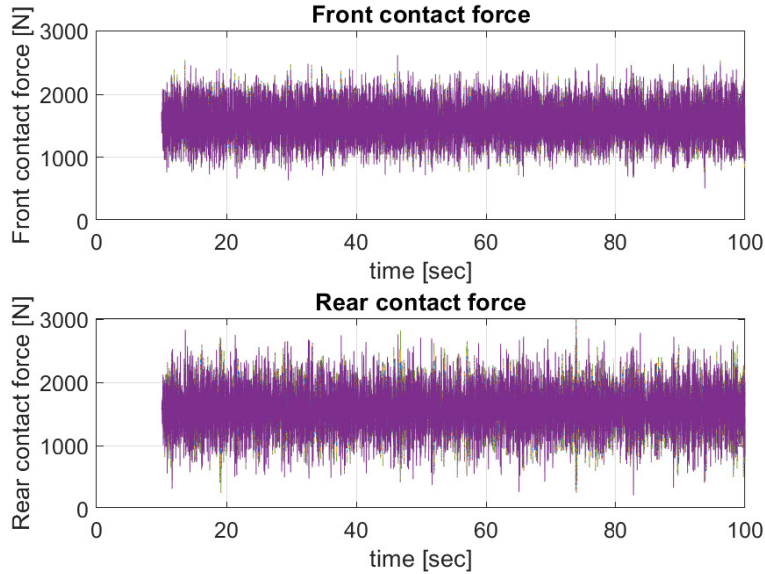


Figure 4.12: Contact forces on tyres during rear sensitivity.

Figure 4.13 and 4.14 shows the 3d sensitivity stiffness-damping sensitivity for vertical and pitch cost functions.

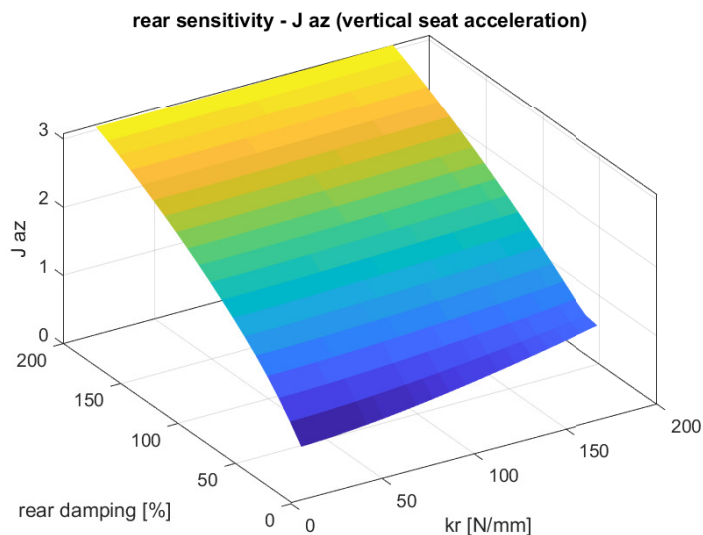


Figure 4.13: Rear sensitivity J_{az} .

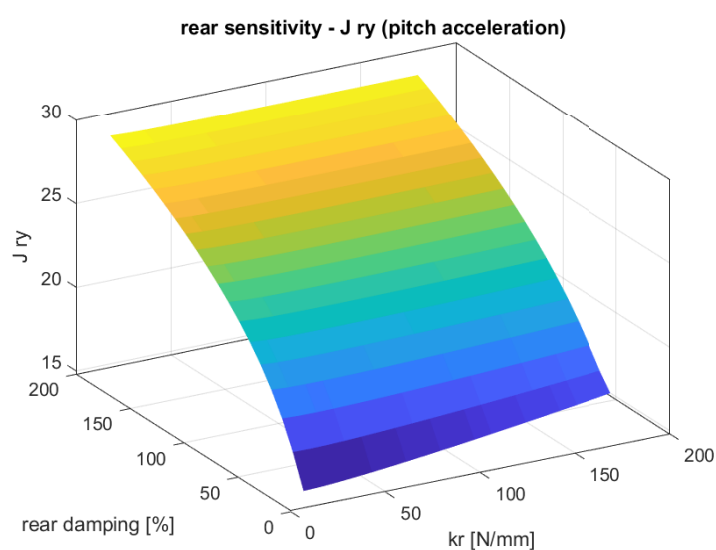


Figure 4.14: Rear sensitivity J_{ry} .

Figure 4.15 and 4.16 shows the maximum (blue) and minimum (red) change in the cost functions as compared to the nominal stiffness as a function of rear damping scaling factor for vertical (J_{az}) and pitch (J_{ry}) cost functions respectively. As seen from figure 4.15, the vertical cost function has a massive change in cost function in low damping whereas the pitch cost function (figure 4.16) range has a medium change in cost function even in low damping. The range of relative change in both vertical and pitch cost function drops sharply after a 40 % damping.

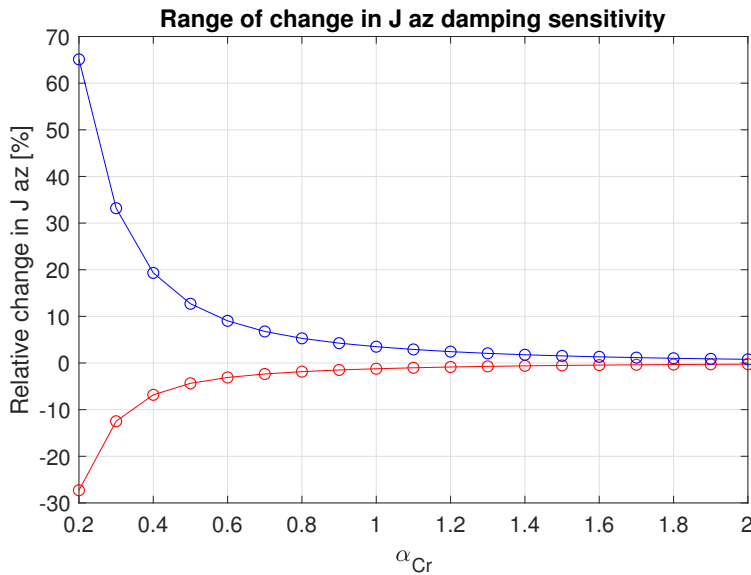


Figure 4.15: Rear J_{az} stiffness sensitivity range with different dampings.

Thus it can be concluded that in order to notice any improvement in comfort using a variable stiffness algorithm, it is imperative to reduce the damping. The rear suspension shows a higher span of cost function (J_{az} in particular) and hence it is more suitable for the multichamber optimization.

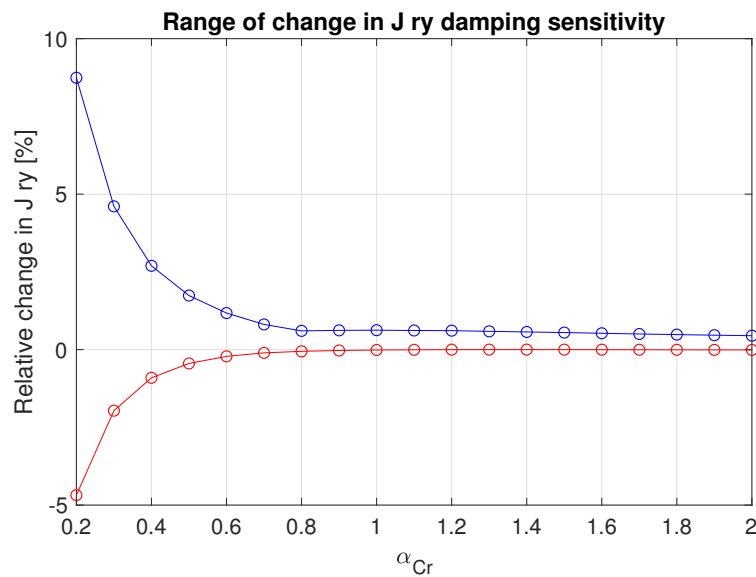


Figure 4.16: Rear J_{ry} stiffness sensitivity range with different dampings.

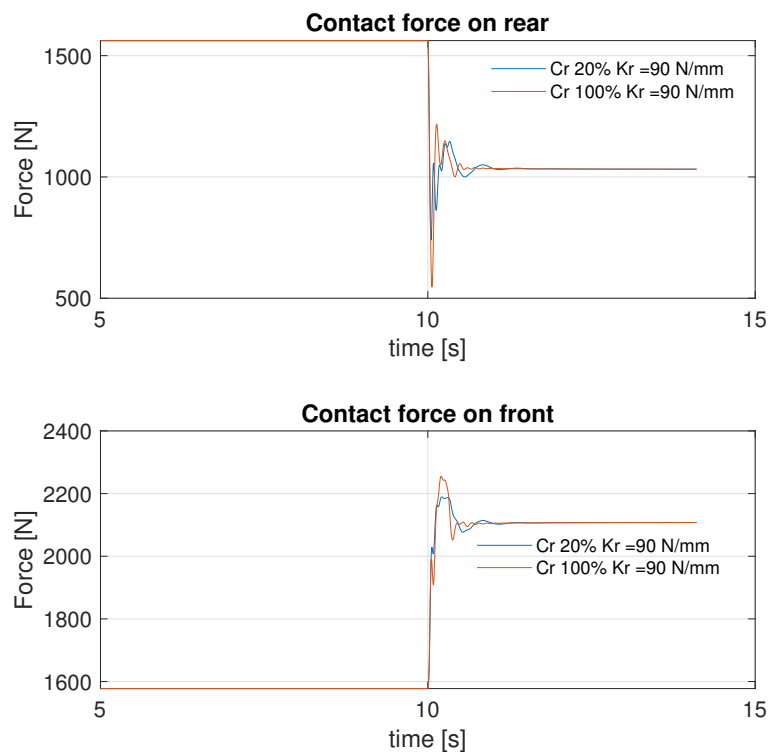


Figure 4.17: Contact forces on tyres during braking maneuver.

4.3 Effect of damping on longitudinal dynamics

From the previous section, it was noticed that the rear suspension is more suitable for observing the improvement in comfort using a variable stiffness at low damping only. In order to check whether the lowered damping is a reasonable representation of longitudinal dynamics, a braking maneuver is performed with the nominal and low damping as shown in figure 4.17. The dynamical response of the braking maneuver show that reducing the damping gives a very similar longitudinal behaviour than the nominal damping. The rear contact force amplitude change is even lower in reduced damping than in the nominal damping.

4.4 Conclusion

As observed from the front and rear analysis of the suspension, it is clear that the nominal damping of motorcycle is too high to modulate the stiffness in order to improve the comfort significantly, as a result the damping must be reduced. At low damping, the range of change in pitch acceleration for the front and rear suspension is similar to each other. Although for vertical acceleration, the range in the rear suspension is much higher than the front suspension. Since a higher range permits for a higher allowability to improve the comfort, thus the rear suspension is suitable for a stiffness modulation to improve the comfort at low damping rather than using the front suspension.

As previously recalled, to compute the total comfort cost function - as presented in figure 3.11 - the vertical and pitch accelerations must be normalized with respect to the value assumed in a nominal scenario. According to the presented analysis, the selected nominal scenario is the one where $\alpha_{cr} = 0.2$. The normalisation factors turns out to be $W_{\text{vertical acc}} = 1$ and $W_{\text{pitch acc}} = \frac{1}{25}$.

Chapter 5

Multichamber sizing

In this chapter, the sizing of multichamber is discussed. A dual chamber suspension is needed to be designed in order to create the 2 stiffness state air-spring. Firstly the parameters to be determined are discussed. Then the equations involving the multichamber suspension parameters are expanded and reformulated. Finally, a parameter sensitivity is performed with the reformulated equations to design the multichamber size.

5.1 Model

The multichamber suspension model has been previously discussed in chapter 3. The stiffness of the multichamber suspension depends on the pressure, volume and area of the suspension given by equation 3.7. The dynamical pressure equations of the main and auxiliary chamber is given by equation 3.9.

5.2 Sizing objective

The 4 unknowns needed to size the multichamber are the following:

1. Pressure preload, p_0

2. Radius of piston, r
3. Height of nominal chamber, h
4. Volume of the auxiliary chamber, V_{aux}

Area of the piston, $A_m = \pi r^2$ and volume of the nominal chamber, $V_0 = \pi r^2 h$.

The dimensions of the multichamber suspension are represented by figure 5.1.

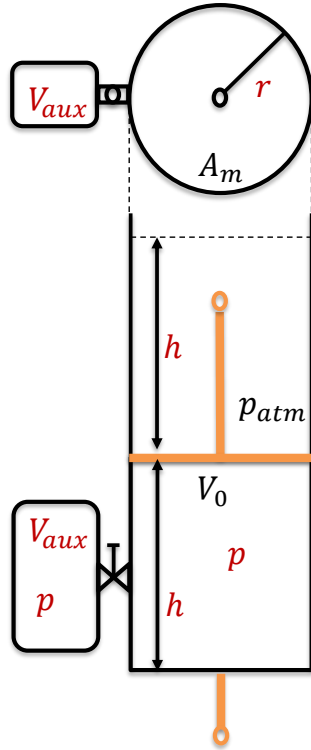


Figure 5.1: Multichamber suspension dimensions.

5.3 Equations of the multichamber suspension

The relationship between the multichamber parameters and suspension equivalent parameters are discussed in this section. A constraint on height of nominal chamber, $h < 65$ mm is set due to the limited physical space of a practical motorcycle suspension. Equation 5.1 represents the relationship between pressure

(p_0) and preload force, where p_{atm} is the atmospheric pressure.

$$F_{preload} = (p_0 - p_{atm})A_m^2 \quad (5.1)$$

The two stiffness of this suspension k_{high} and k_{low} are expressed using equations 5.2 and 5.3 respectively, where n is the polytropic index of air.

$$k_{high} = \frac{p_0 n A_m^2}{V_0} \quad (5.2)$$

$$k_{low} = \frac{p_0 n A_m^2}{V_0 + V_{aux}} \quad (5.3)$$

As $A_m = \pi r^2$ and $V_0 = \pi r^2 h$, equations 5.1 and 5.2 can be rewritten as equations 5.4 and 5.5 respectively. The r and h corresponds to the radius and height of the suspension.

$$F_{preload} = (\textcolor{red}{p_0} - p_{atm})\pi \textcolor{red}{r}^2 \quad (5.4)$$

$$k_{high} = \frac{\textcolor{red}{p_0} n \pi \textcolor{red}{r}^2}{h} \quad (5.5)$$

5.4 Parameters sensitivity

The number of unknowns are 4 (p_0, r, h, V_{aux}) and number of equations are 3 (5.1,5.4,5.5). A tri-sensitivity using equations 5.4 and 5.5 is done in figure 5.2 which shows the height of the nominal chamber as a function of preload pressure and radius. As the radius decreases, then the height also decreases. It is desirable to have a smaller size due to the limited space in a motorcycle. On the other hand, decreasing the height and radius greatly gives rise to a very large preload pressure which the walls of the chamber might not sustain.

The optimum triplet of p_0, r and h is selected by imposing the height constraint and highlighted by the red dot in figure 5.2. The optimal values are substituted back in equation 5.3 to obtain the auxiliary chamber volume, V_{aux} .

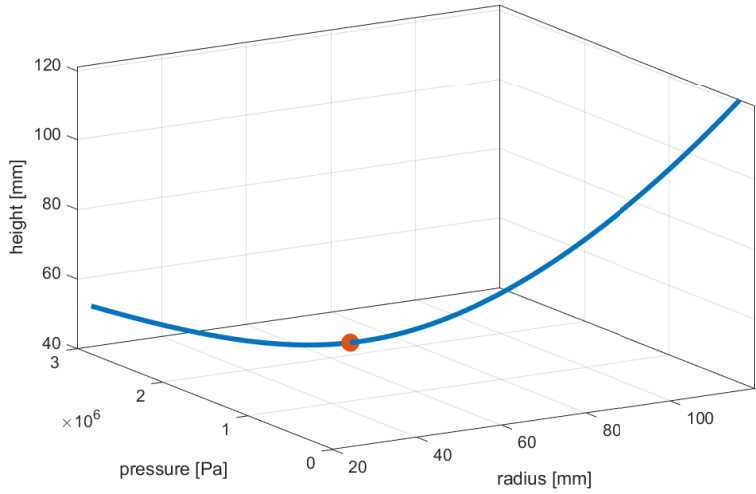


Figure 5.2: Tri-sensitivity for multichamber sizing

5.5 2 state stiffness selection

The comfort of the motorcycle with a variable stiffness switching needs to be assessed in this thesis so different multichamber suspensions need to be explored.

The higher stiffness is kept as the nominal stiffness of the rear suspension while the lower is changed. In total 7 multichamber suspensions are designed with the configurations shown in table 5.1, where $\Delta k = k_{high} - k_{low}$.

Δk [N/mm]	k_{high} [N/mm]	k_{low} [N/mm]
75	90	15
60	90	30
45	90	45
30	90	60
15	90	75
10	90	80
5	90	85

Table 5.1: Stiffness configurations for multichamber suspension

5.6 Sizing results

The common parameters for all the sized multichamber suspensions from table 5.1 is given in table 5.2 since they have the common k_{high} . The auxilary chamber, V_{aux} varies with k_{low} as shown in figure 5.3.

Parameter	Value	Units
p_0	7.84	bar
r	40	mm
h	59.6	mm

Table 5.2: Multichamber sized parameters

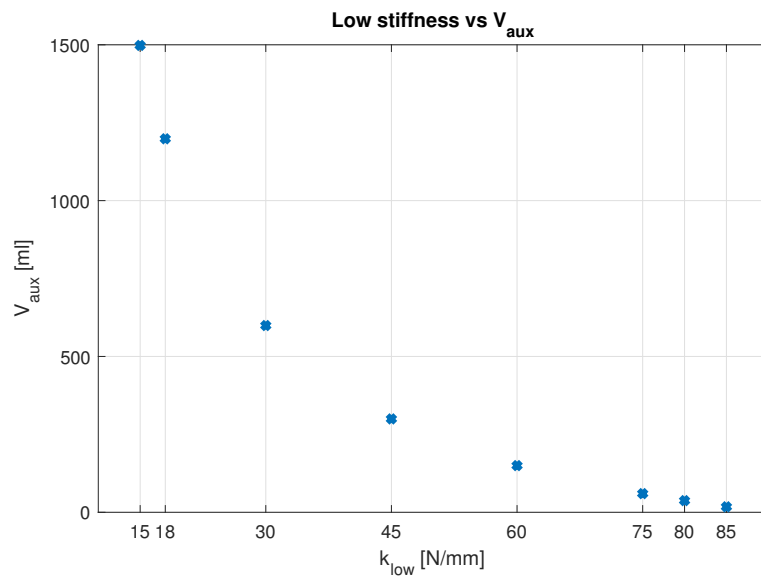


Figure 5.3: k_{low} and V_{aux} relationship

5.6.1 Comparing sizing with a real suspension

Comparing the length and radius

We can compare the dimensions with a motorcycle rear suspension available in the market by taking the example of Ohlins SP36PL. The suspension's can be seen in figure 5.4. The maximum extended length of this suspension is $L_{sus} = 355mm$ and the diameter is $D_{sus} = 36mm$. This compares with the sized multichamber suspension as it is sized with an extended length of $2*h = 119.2mm$ and diameter of $2 * r = 80mm$.

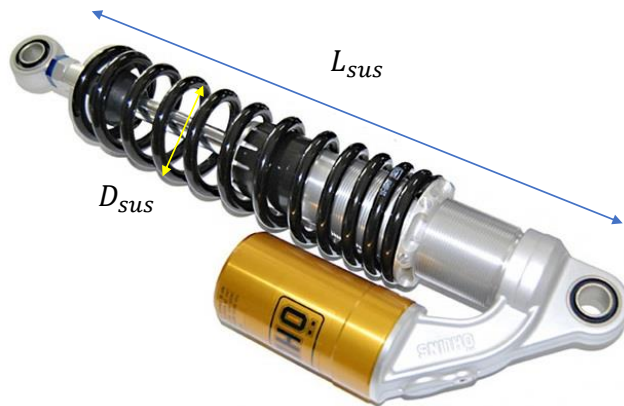


Figure 5.4: Ohlins SP36PL

Comparing the preload pressure

The Ohlins MTB TTX2 (shown in figure 5.5) is a mountain bike air spring suspension. It has a maximum pressure handling of 17.2 bar. The preload pressure used for sized multichamber is $p_0 = 7.84$ bar which is well below the maximum value.



Figure 5.5: Ohlins MTB TTX2

5.7 Conclusion

A sizing strategy was demonstrated for motorcycles and 7 different multichamber suspensions are sized in this chapter. In order to assess the improvement of comfort, the brute-force optimization algorithm is performed using these 7 multichamber suspensions on the rear wheel in the next chapter.

Chapter 6

Brute-force optimization

This chapter talks about the brute-force optimization algorithm implementation with the multichamber suspension. The algorithm working is first discussed and then the parameters are set for optimization. The results of the optimization with the 7 sized multichamber suspensions are discussed subsequently.

6.1 Brute-force optimization algorithm

The brute-force optimization algorithm is used to benchmark the maximum improvement in comfort. The multichamber valve status is optimized upto T_f , final time. The amount of time the stiffness is constant in a sequence is given by T_r (stiffness refresh time). In each optimization time window there are Q stiffness configurations. The optimization time window length is given by $T_w = Q * T_r$. In each optimization time window the number of sequences simulated are 2^Q since there are only 2 stiffness possible here.

Initially the motorcycle starts off with $t=0$. The motorcycle is simulated upto $t = T_w$ for all possible stiffness sequences (2^Q) as shown in figure 6.1. The optimal cost-function is selected and the first stiffness configuration of the corresponding sequence is stored in the optimal sequence as shown in figure 6.2.

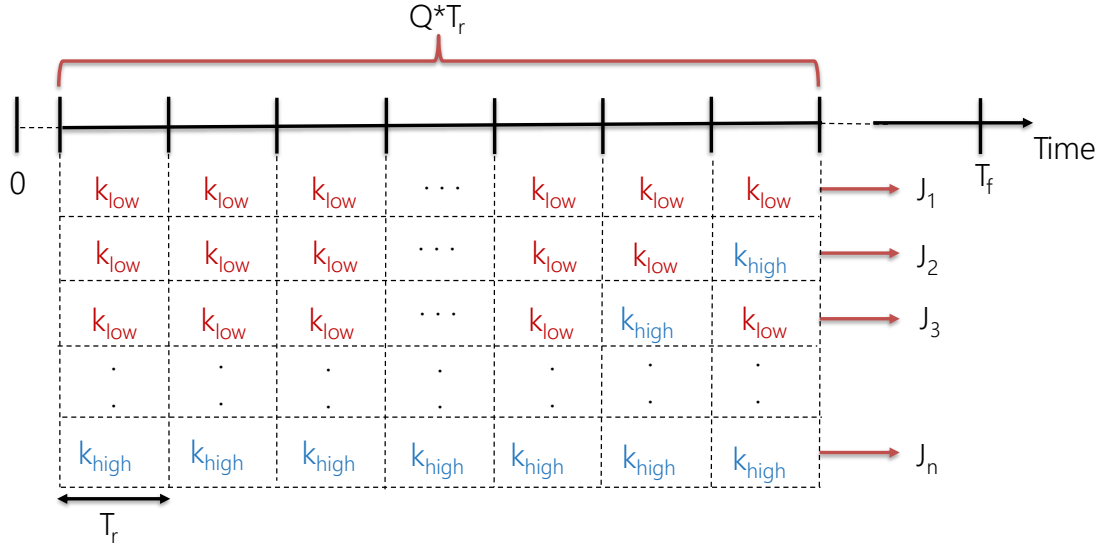


Figure 6.1: Brute-force optimization algorithm

The optimization time-window is shifted by T_r and the optimization is repeated

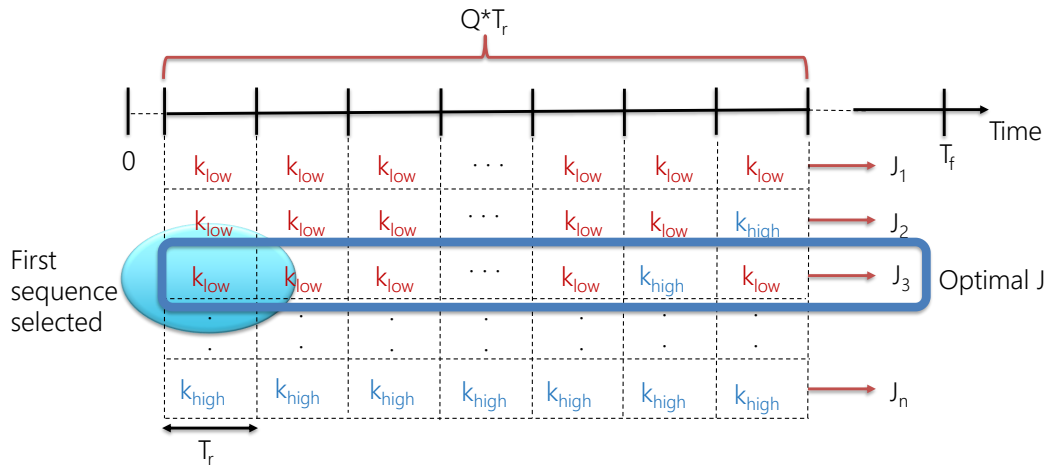


Figure 6.2: Selection of optimal stiffness

by simulating the motorcycle from $t = 0$ upto $t = T_w + T_r$ to find the next optimal stiffness configuration as shown in figure 6.3.

In this manner, the optimization time window keeps shifting upto the final simulation time T_f and the complete optimal sequence is recorded.

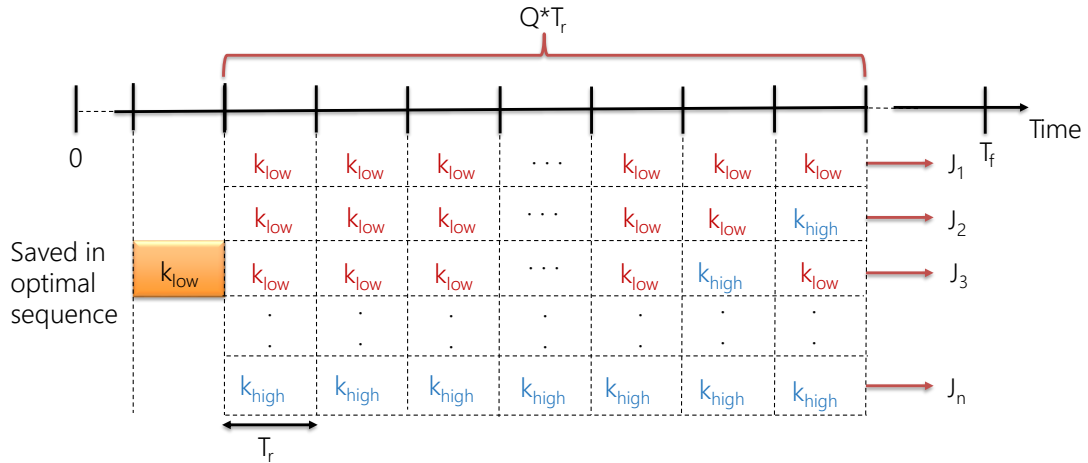


Figure 6.3: Shifting the optimization horizon

6.1.1 Optimization conditions

The J_{tot} cost function (defined in chapter 3) will be used for the purpose of optimization. The $T_f = 2s$ is selected due to the computational time taken to do the entire optimization.

The stiffness refresh time is $T_r = 30ms$. This is done in order to keep a reasonable time that allows for the settling of equilibrium conditions of the multichamber states.

$Q = 10$, as this number of stiffness configurations in each sequence led to good results with quarter car optimization conducted in previous work. A total of $2^{10} = 1024$ sequences will be simulated in each time window (T_w).

The stiffness used are 2 state as defined from table 5.1. The motorcycle speed is 90 kmph simulated on class A road profile.

6.2 Optimization results

The brute-force optimization algorithm is performed using 7 different multichamber suspension as sized in chapter 3 given by table 5.1. The passive k_{low} (soft) configuration simulations are used in order to compare with the optimal results.

The comfort cost functions of both passive soft and optimal sequence are plotted in figure 6.4 as a function of the span of stiffness used in optimization.

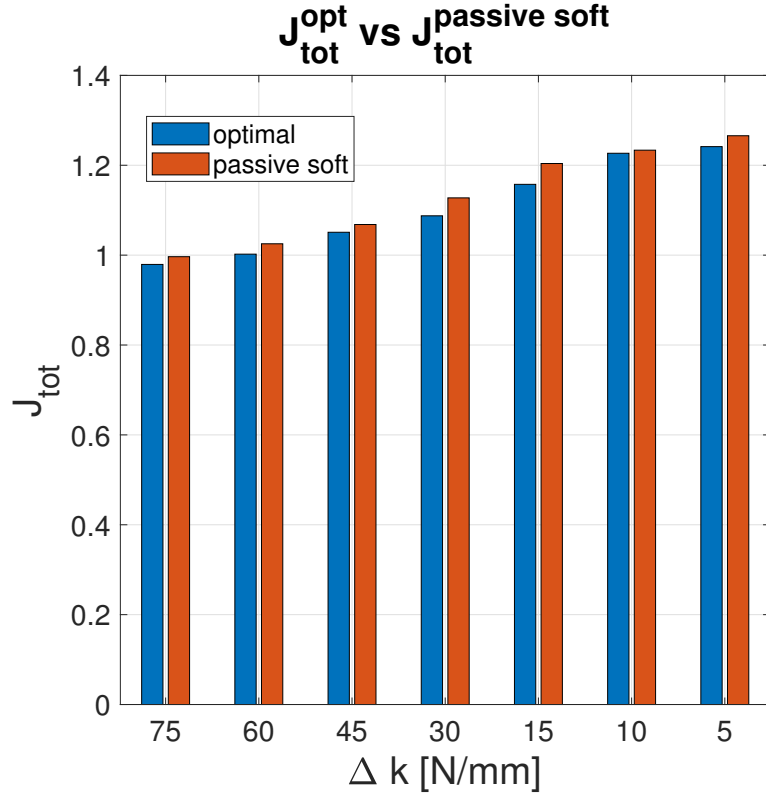


Figure 6.4: Brute-force optimization result compared with passive

$$J_{tot} \text{ relative} = \frac{J_{tot}^{opt} - J_{tot}^{soft}}{J_{tot}^{soft}} \quad (6.1)$$

The improvement of cost function from the passive to optimal can be described using a relative change. The relative change in cost function is computed by equation 6.1, where J_{tot}^{soft} is the cost function obtained using the passive soft and J_{tot}^{opt} is the cost function obtained using the optimal sequence. Figure 6.5 shows the relative change in cost functions due to optimization as a function of the span of stiffnesses used in optimization.

The interesting result reached is that a higher span used for optimization does not necessarily give rise to a higher improvement in comfort. The span $\Delta k =$

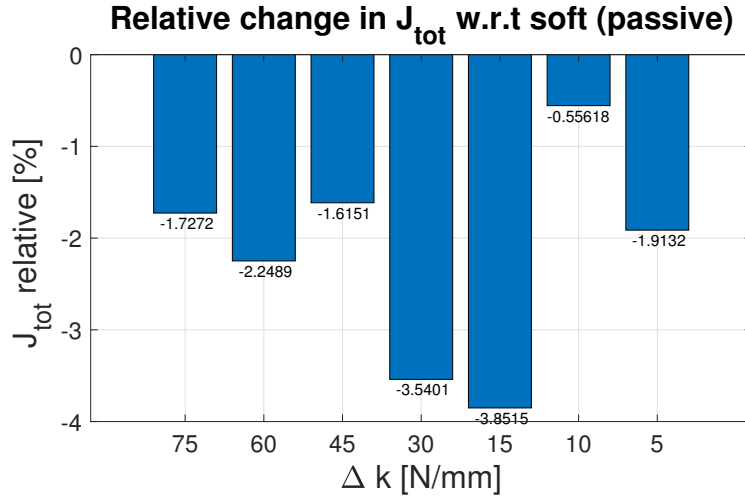


Figure 6.5: Relative change in optimal comfort with respect to passive soft

$15N/mm$ gave rise to the maximum improvement in comfort when compared with the passive soft stiffness configuration.

While comparing with the soft stiffness comfort gives the control benefit, the soft stiffness cannot be used in a real environment due to hitting the end stops. The relative change in optimal cost function with respect to passive normal configuration can be computed using 6.2. A relative change in cost function as a function of stiffness span is plotted in figure 6.6. Since the cost function value of the normal passive stiffness configuration (J_{tot}^{normal}) is the largest when compared to any of the optimal ones, the graph is linearly decreasing. The change in comfort cost function with respect to the normal stiffness configuration is proportional to the span of the stiffness used in optimization.

$$J_{tot} \text{ relative} = \frac{J_{tot}^{opt} - J_{tot}^{normal}}{J_{tot}^{normal}} \quad (6.2)$$

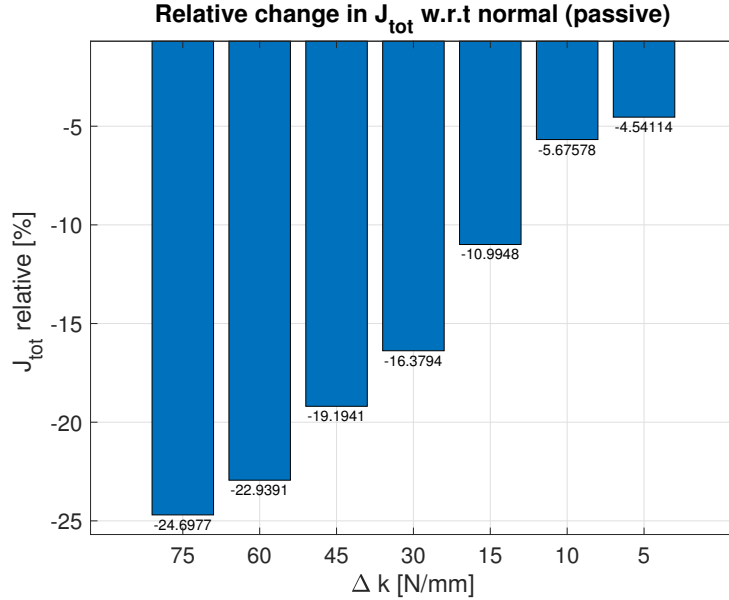


Figure 6.6: Relative change in optimal comfort with respect to passive normal

6.3 Contribution of vertical and pitch acceleartion improvement

As discussed in the previous section, the optimization was performed with the J_{tot} cost function. In order to find the contribution of the vertical acceleration towards the total cost function improvement, we can compute the vertical acceleration cost function using the previous optimal sequence (J_{az}^{opt}) and compare the relative change with the vertical acceleration cost function using passive soft spring (J_{az}^{soft}). The relative change in improvement of vertical acceleration (J_{az} relative) is given by equation 6.3. This relative change quantifies the contribution of the vertical acceleration in improving the J_{tot} cost function during optimization.

$$J_{az} \text{ relative} = \frac{J_{az}^{opt} - J_{az}^{soft}}{J_{az}^{soft}} \quad (6.3)$$

Similarly, the relative change in improvement of pitch acceleration ($J_{ry\text{ relative}}$) is given by equation (6.4) where the J_{ry}^{opt} is the pitch cost function computed using the previous optimal sequence and J_{ry}^{soft} is the pitch cost function computed using the passive soft spring.

$$J_{ry\text{ relative}} = \frac{J_{ry}^{opt} - J_{ry}^{soft}}{J_{ry}^{soft}} \quad (6.4)$$

Figure 6.7 shows the contributions of the vertical and pitch accelerations improvement as a function of the span of stiffness used in optimizations. It is observed that using a high span stiffness, the pitch cost function reduction contributes more towards the total comfort improvement. While if we use a stiffness span in between the maximum and minimum, the vertical acceleration reduction leads to the overall improvement of the comfort.

6.4 Conclusion

At first sight the result of the optimization is counter intuitive, usually when we have a large control authority, we can achieve better improvement. In this case we don't have a control authority range but rather we are switching between the two values of stiffness so the comfort improvement is not the greatest in a larger span of the stiffness but in a span that is in between the maximum and minimum value.

The use of a high span for optimization doesn't lead to a bigger improvement when compared to the passive additionally because the high span multichamber suspension uses also the softest spring. The softest spring is already the best from a comfort point of view, so the multichamber algorithm finds it difficult to out perform its comfort. On the other hand, if we use a low stiffness which is not too low in the multichamber, then the algorithm finds room to improve as compared to the passive low stiffness case.

The passive lowest stiffness is not ideal to be used in a real motorcycle due

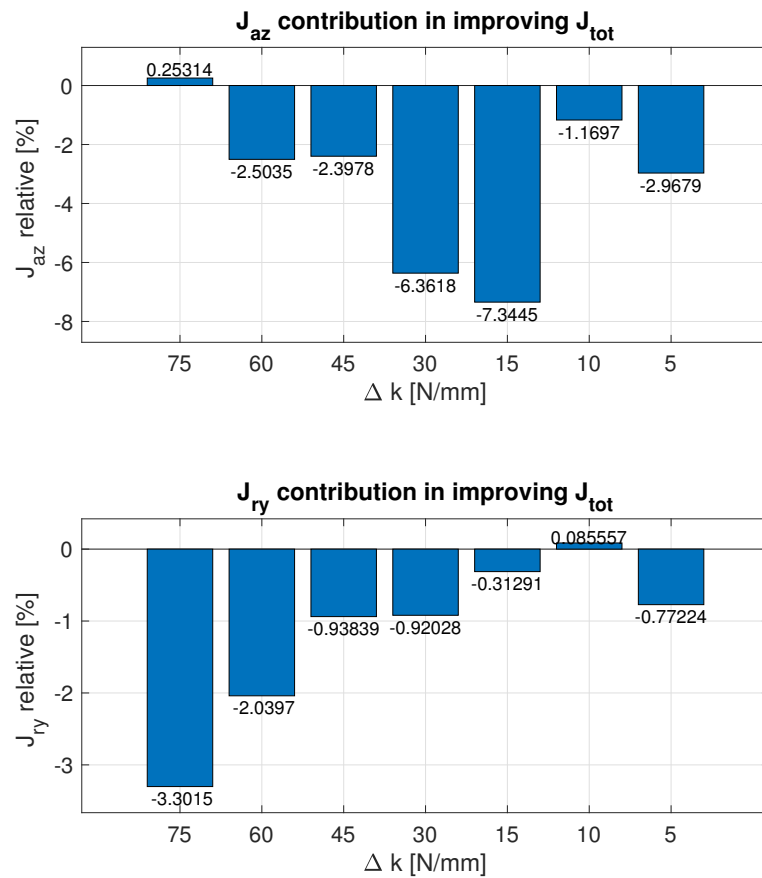


Figure 6.7: Vertical and pitch acceleration contribution in improving the overall cost function

to its likelihood of hitting the endstops easily. Even though the multichamber suspension with the maximum span gives rise to the lowest cost function, from the sizing point of view it is not ideal as it requires an auxiliary chamber size of 1.5 L. The multichamber suspension with a medium span on the other hand would require an auxiliary chamber size of 60 mL only and give the maximum control benefit at the same time. So the multichamber suspension with the medium span provides a better comfort-sizing tradeoff as well.

Chapter 7

Conclusion

The aim of the thesis is analyzing the potentials of a multichamber suspension in a more realistic vehicle application rather than the quarter-car model. To do so the optimal control of the suspension has been implemented following a brute-force optimization approach.

The state of the art stiffness control architectures along with stiffness control algorithms are outlined in chapter 2. This showed the growing research in variable stiffness technology and the potential benefits of multichamber suspension over the other existing ones. The motorcycle parameters and simulation model are described in chapter 3. The comfort cost function was also defined appropriately weighting the vertical and pitch accelerations. The passive stiffness and damping sensitivity was carried out in chapter 4. From the sensitivity analysis, the potential to improve comfort by modulating stiffness was observed in low damping on the rear suspension. In chapter 5, the sizing procedure for a dual stiffness multichamber suspension was discussed using different stiffness combinations. Seven multichamber suspensions were sized whose size was comparable to that of suspensions in the market.

These multichamber suspensions were then used to perform the brute-force optimization on the motorcycle to improve the ride comfort in chapter 6. The

optimization gave rise to an interesting result that maximum control benefit was seen in a medium stiffness span rather than a high stiffness span of the multichamber configurations. Additionally, from the sizing-comfort tradeoff point of view, the medium stiffness span multichamber is better than the high stiffness span multichamber.

Some directions for future work related to the thesis are suggested:

- We can perform the same multichamber optimization setup on different road profiles to verify if same result holds true.
- Interpret any control laws from the optimization results
- Combine damping and stiffness switching in brute-force optimization in order to see the effect of combined switching.

Bibliography

- [1] M. Agostinacchio, Donato Ciampa, and Saverio Olita. The vibrations induced by surface irregularities in road pavements – a matlab® approach. *European Transport Research Review*, 6:267–275, 09 2013.
- [2] S. Dattilo, G. Panzani, M. Corno, and S. Savaresi. On optimal control of multichamber suspensions. *IFAC*, 2020.
- [3] W. Li H. Du and N. Zhang. Semi-active variable stiffness vibration control of vehicle seat suspension using an mr elastomer isolator. *Smart Mater*, 2011.
- [4] S. Singh L. Jugulkar and S. Sawant. Analysis of suspension with variable stiffness and variable damping force for automotive applications. *Advances in Mechanical Engineering*, 2016.
- [5] R. Lenain M. Deremetz and Benoit Thuilot. Stiffness and damping real-time control algorithms for adjustable suspensions : A strategy to reduce dynamical effects on vehicles in off-road conditions. *IFAC-PapersOnLine*, 50(1):1958–1964, 2017. 20th IFAC World Congress.
- [6] D. R. Patel O. M. Anubi and C. D. Crane III. A new variable stiffness suspension system: passive case. *Mech. Sci.*, 4, 139–151, 2013.
- [7] C. Spelta, F. Previdi, S. M. Savaresi, P. Bolzern, M. Cutini, and C. Bisaglia. A novel control strategy for semi-active suspensions with variable damping

- and stiffness. In *Proceedings of the 2010 American Control Conference*, pages 4582–4587, 2010.
- [8] T. Mizuno Y. Ishino and M. Takasaki. Stiffness control of magnetic suspension by local current feedback. *Proceedings of the European Control Conference*, 2009.